RTG "Functionalization of Semiconductors"

Seminar 2013

Schloss Bettenburg, Hofheim/Unterfranken, 19.08.2013 – 22.08.2013

Research Summaries

Graduiertenkolleg „Funktionalisierung von Halbleitern“

Seminar 2013

19. – 22.08.2013, Seminarzentrum Schloss Bettenburg, Hofheim

Program:

19.08.2013

until 12:30	Arrival
12:30 – 14:30	Lunch & Opening
14:30 – 16:00	Presentations (Chair: Ingo Meyenburg)
	Uwe Kaiser: Multiplexed Measurements by Time Resolved Spectrocopy using Colloidal CdSe/ZnS Quantum Dots
	Nils Rosemann: Long-Term Stability of Tin/Sulfur Clusters under UV illumination studied by Time-Resolved Photoluminescence
16:15 – 16:45	Coffee
16:45 – 17:30	Presentation (Chair: Peter Ludewig)
	Phil Rosenow: Computational investigation of the electronic properties of semiconductor laser materials and the thermodynamic properties of the Si(001)2x1-surface under MOVPE conditions
17:30 – 18:00	Free time
18:00 – 19:30	Dinner

20.08.2013

8:00 – 09:45	Breakfast
09:45 – 10:30	Presentation (Chair: Ronja Woscholski)
	Katharina Werner: Gallium and Carbon Growth for the Direct Chemical Vapor Phase Deposition of Graphene on Si (001)
10:30 – 11:00	Coffee
11:00 – 12:30	Presentations (Chair: Sina Lippert)
	Marcel Reutzel: Adsorption of tetrahydrofuran on the Si(001) surface studied by means of STM, XPS, and UPS
	Alexandra Ostapenko: Preparation and characterization of phenylphosphonic acid self-assembled monolayers on ZnO substrates
12:30 – 14.30	Lunch
Afternoon	Hiking: To the Schwedenschanze, over Rottenstein and Reckertshausen to Hofheim, Dinner in the „Fränkischer Hof“

21.08.2013

8:00 – 09:45	Breakfast
09:45 – 10:30	Postertalks (Chair: Phil Rosenow), Postersession & Discussions
10:30 – 11:00	Coffee
11:00 – 12:30	Postersession & Discussions (continued)
12:30 – 14.30	Lunch
14:30 – 16:00	Presentations (Chair: Eliza Leusmann)
	Jens Eußner: Formation, Sysnthesis and Characterization of Binary and Ternary Functionalized Chalcogenidometallate Complexes
	Nikolai Knaub: STEM Annular Dark Field Measurements of III/V Semiconductors
16:00 – 16:30	Coffee
16:30 – 18:00	Organization (discussion about schedules, election of new student speaker) and free time
18:00 – 19:30	Dinner

22.08.2013

8:00 – 09:45	Breakfast
09:45 – 10:30	Presentation (Chair: Benjamin Breddermann)
	Jan-Oliver Oelerich: Advanced percolation description of variable-range-hopping
10:30 – 11:00	Coffee
11:00 – 11:45	Closing remarks
12:00 – 14:00	Lunch
	Departure

Posters

1. Marcus Lipponer: Adsorption Dynamics of Tetrahydrofuran on Si(001)
2. Eliza Leusmann: Towards Connection of Chelating Ligands and Rutthenium Complexes to Tin/Sulfur Clusters
3. Ronja Woscholski: Optical and electrical properties of GaNAsP-QW materials
4. Sina Lippert: Four-wave mixing
5. Andreas Stegmüller: Modeling MOVPOE Growth of GaP on Si(001) by DFT: Gas Phase Decomposition to Thin Layer Structures
6. Nadeem Sabir: Synthesis and characterization of Mn-CsD/ZnS Nanoparticles
7. Christian Prinzisky: Coordination Chemistry and Redox Activity of Anthraquinone-Based Ligands for Dye-Sensitized Solar Cells
8. Bastian Weinert: Synthesis of ternary intermetalloid cluster
9. Peter Ludewig: MOVPE Growth of Dilute Bismide Ga(AsBi) Quantum Well Structures for High Efficiency IR Laser Devices
10. André Pick: Selective Nucleation of Organic Semiconductors
11. Lars Finger:
12. Ingo Meyenburg: Optical Spectroscopy on planar ZnO/Pentacene Hybrids
13. Benjamin Breddermann: Bandstructure, gain and photoluminescence of dilute bismide semiconductors

Computer simulation of growth kinetics of lattice-matched semiconductor compounds

Jan Oliver Oelerich

Faculty of Physics and Material Sciences Center, Philipps-Universität Marburg

Introduction

In experimental studies of epitaxial growth (MOVPE) of gallium phosphide (GaP) on silicon (Si) 001 surface, a significant intermixing of the two materials at their interface is observed: In the first six to eight layers of GaP on the substrate, a decreasing amount of silicon is found, that forms pyramidal structures. The result was obtained using transmission electron microscopy techniques. A schematic view of the silicon concentration at the interface is shown in Fig. 1, in which the bright hexagons indicate higher silicon concentrations. Clearly, a significant amount of intermixing between GaP and Si is present at the interface.

Since the silicon substrate surface is rather flat before the growth, the observed intermixing must be a result of the growth procedure. One possible reason for such effects is lattice strain: When the two materials forming the interface do not share the same lattice constant, i.e., are not *lattice-matched*, the lattice atoms of both materials experience strain forces and are displaced from their equilibrium positions. This leads to clustering on the surface during crystal growth, as for instance studied in Ref. [1] for germanium on silicon. However, the diamond cubic structures of GaP and Si are almost lattice-matched, which rules out lattice strain as possible driving force of the observed intermixing. To our knowledge, the literature does not provide any other mechanisms or studies responsible for interface intermixing. Therefore, new theories must be proposed and checked.

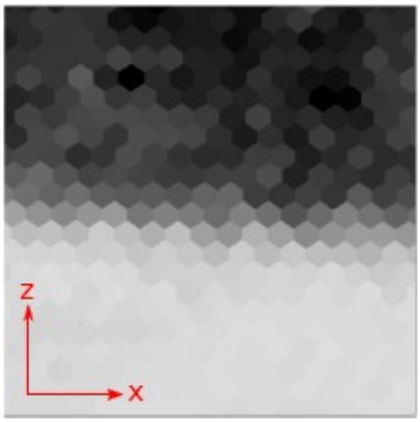

Fig. 1: Schematic view of experimental observation of the intermixing phenomenon at the Si-GaP interface. The bright hexagons indicate the silicon concentration within the material. The growth direction is z.

One of the possible mechanisms could be intermixing because of the growth kinetics. During epitaxial growth, new atoms arrive at the surface slowly compared to typical times of surface diffusion processes. Mixture of atomic species may, in addition to Coulomb forces, influence the binding energies decisive for the diffusion kinetics. Hence, the surface may be reconstructed during the growth procedure which could lead to formation of clusters or a roughening of the interface layers.

In order to investigate this theory, we developed a kinetic Monte Carlo (kMC) simulation that is capable of modeling diffusion and growth processes of materials with diamond cubic crystal structure. The simulation is expected to provide a deeper insight into the dynamical behaviour of surface atoms during crystal growth.

Method

A standard kinetic Monte Carlo algorithm [1,2] is implemented to study growth kinetics and surface diffusion of materials with diamond cubic crystal structure. The simulation supports the following physical events:

- **Diffusion**: An atom jumps to nearest- or second-nearest-neighbor site.
- **Adsorption**: A new atom arrives at a random surface site. This is used to simulate growth.
- **Desorption**: An atom is thermally desorbed from the surface and leaves the simulation.
- **Atom exchange**: Nearest-neighbor atoms exchange lattice positions.

The rates of these events depend on several parameters: Nearest-neighbor and second-nearest-neighbor binding energies between the different atomic species, additional energy barriers caused by lattice topology, growth rates and system parameters (temperature, attempt-to-escape frequency).

In each simulation step, the next event is randomly chosen from the set of possible transitions and executed. Physical time is advanced by the corresponding Δt and the event list is updated for the new configuration. This procedure is repeated until the termination criterion is reached.

Results

Preliminary results prove that interface intermixing during growth can, in principle, be induced by the growth and diffusion kinetics. In Figs. 2 and 3, two example outputs of the simulation procedure are shown. The system snapshots were visualized using the ovito software [3]. In Fig 2 phosphorus atoms are grown on a silicon surface and form pyramidal structures, for which the driving forces are differences in binding energies. The figure proves, that the experimentally observed structures can be caused by atomic interactions during growth. Fig. 3 contains a smaller example system of gallium phosphide on silicon substrate. Here the surface shows a very rough structure in contrast to the flat deposition in Fig. 2.

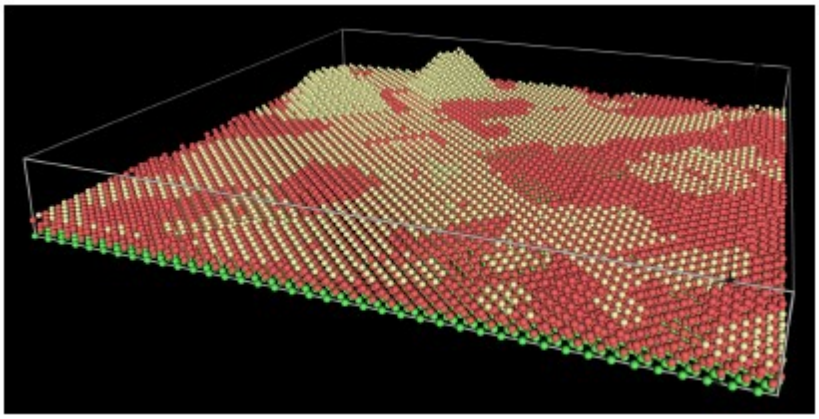

Fig. 2: Pyramidally clustered P (beige atoms) on Si (green and red atoms) substrate, 40 x 40 unit cells. Simulation temperature: 950 K.

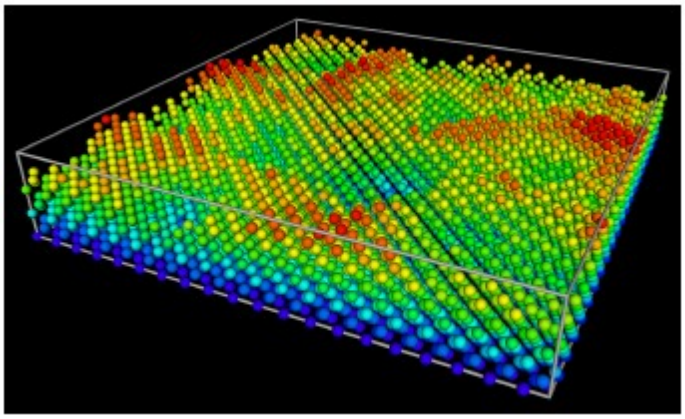

Fig. 3: Height profile of GaP on Si substrate, 20 x 20 unit cells. Simulation temperature: 730 K.

Conclusions and Outlook

So far, we can conclude that kinetic Monte Carlo simulation of growth processes serve as a good candidate for computational studies of crystal growth kinetics. It is a very flexible method and allows for dynamic observation of physical processes at the surface and during crystal growth. It seems suitable to address the physical problem explained in the Introduction.

In future, the parameter space must be narrowed and realistic parameter sets found, in order to allow more physically meaningful simulations. Experimentally observed effects are to be recovered with the simulation or must be included in the code. Significant additional interaction types, for instance coulomb interactions, will allow realistic predicitons.

References

[1] J. V. Smagina, V. a. Zinovyev, a. V. Nenashev, a. V. Dvurechenskii, V. a. Armbrister, and S. a. Teys, Journal of Experimental and Theoretical Physics **106**, 517–527 (2008).

[2] A. P. J. Jansen, *An Introduction To Monte Carlo Simulations Of Surface Reactions* (Springer, Berlin, 2012).

[3] A. Stukowski, Modelling and Simulation in Materials Science and Engineering **18**, 015012 (2010).

Long-Term Stability of Tin/Sulfur Clusters under UV illumination studied by Time-Resolved Photoluminescence

Project B4: Nils Rosemann and Sangam Chatterjee

Optics & Laser Spectroscopy Group – Faculty of Physics, Philipps-Universität Marburg

Tin/Sulphur crystals with various organic ligands form complex crystalline structures with potentially pronounced nonlinear optical properties. One example is second-harmonic generation (SHG) expected in non-centrosymmetric structures. To quantify the SHG one has to ensure that the generated light is not reabsorbed by the crystal. In order to find suitable fundamental and second harmonic wavelength we performed linear absorption measurements on single-crystals made of clusters with an inorganic Sn4S6 core grown in the group of Prof. Dr. Stefanie Dehnen. By choosing suitable ligands, the core rearranges and functionalization of the cluster by attached ruthenium complexes is possible (Fig.1). The use of ruthenium complexes opens a variety of applications, such as dye-sensitized solar cells and chromophores1. Because of rather thick crystals the dynamic range of the absorption setup was too small to provide good-quality measurements. We are currently increasing the dynamic range by using lock-in technique.

Another requirement for efficient energy conversion is the robustness to high electric fields and high-energy photons common to nonlinear optical conversion processes. To investigate the robustness, we perform time-resolved photoluminescence (TRPL) studies on these crystals.

In preliminary work we find a pronounced and irreversible change in the PL spectra and transients following long-term irradiation of similar clusters based on the same core. These changes occurred after illuminating the crystals with 355 nm fs-pulsed laser with high excitation density of ~30 W/cm^2 and short exposure times of 30 s shown in Fig. 2.

Now, we study if these changes also occur in ruthenocene-functionalized clusters. As these clusters tend to degrade under ambient conditions, they are stored and measured in a controlled nitrogen-gas environment. Again, we observe changes in the PL spectra and their transients after high-intensity illumination, as shown in Fig. 4b. These changes are either due to the high peak electric fields of the impinging short pulses or due to the integrated number of high-energy photons. To identify the nature of the photo-induced changes we performed long-term irradiation measurements with low excitation density of ~1 W/cm^2 before high density excitation. Results are shown in Fig. 3.

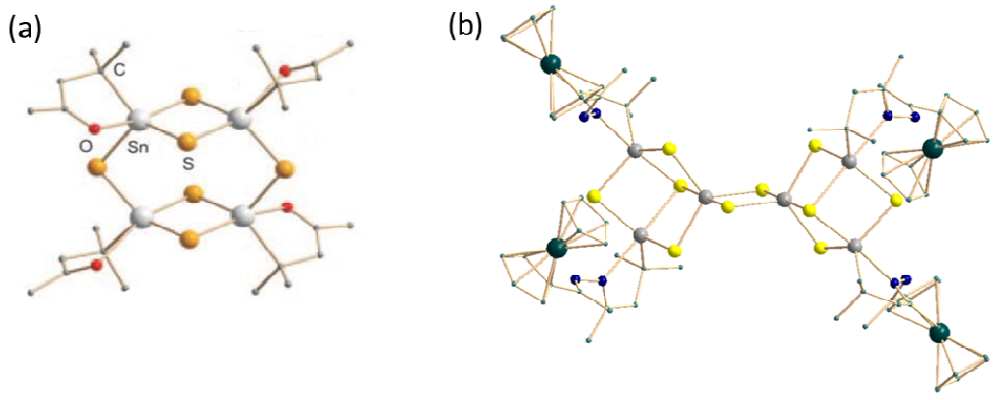

*Figure 1: [(RSn)4S6](R=**CMe2CH2COMe**) cluster core (a)1. Rearanged core with attached hydrazine-derivatized ruthenocene (b)[1].*

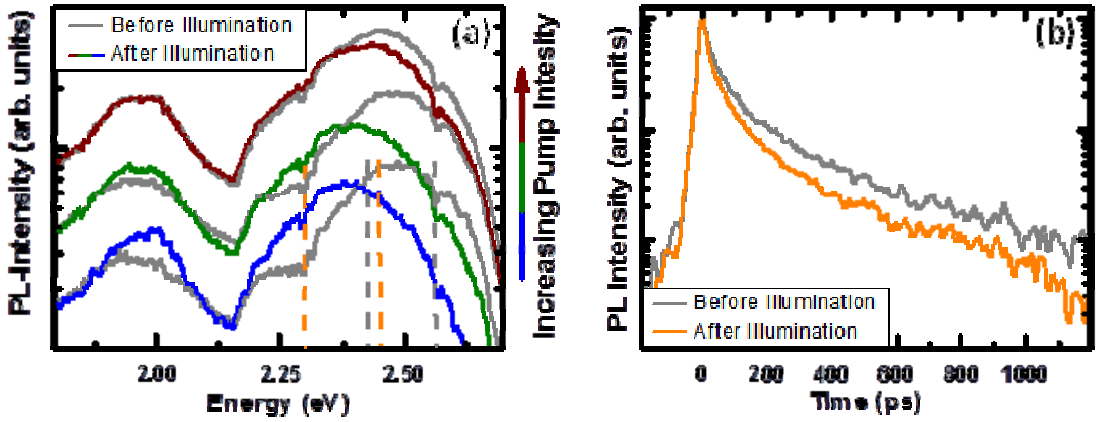

Figure 2: PL spectra of Sn/S cluster single crystals, before and after illumination with high excitation density (a). Transients of the high energy PL peak for lowest pump power (b).

During the first 3h of the low density measurements the integrated PL-Intensity increases. This increase is accompanied by enhanced PL-emission at the low energy side of the peak. Consecutively, the overall intensity decreased by about 50 % on a time scale of one day. The transients show a decrease in decay time over the whole time range as shown in Fig. 4a. Also taking into account the observed intensity decrease this indicates the formation of additional non-radiative recombination channels in the crystal. As these changes appear on a long time scale they are presumably only of chemical nature. The first increase of PL-Intensity might be due to dissociating solvent. This solvent is known to be trapped inside the crystals during growth in solution. The slow decrease in intensity, however, might be caused by chemical degradation of the surface. To validate these two statements, measurements under vacuum conditions are planned. In this case the dissociation of the solvent should be faster as the solvent evaporates faster. The degradation of the surface, however, is expected to be slower.

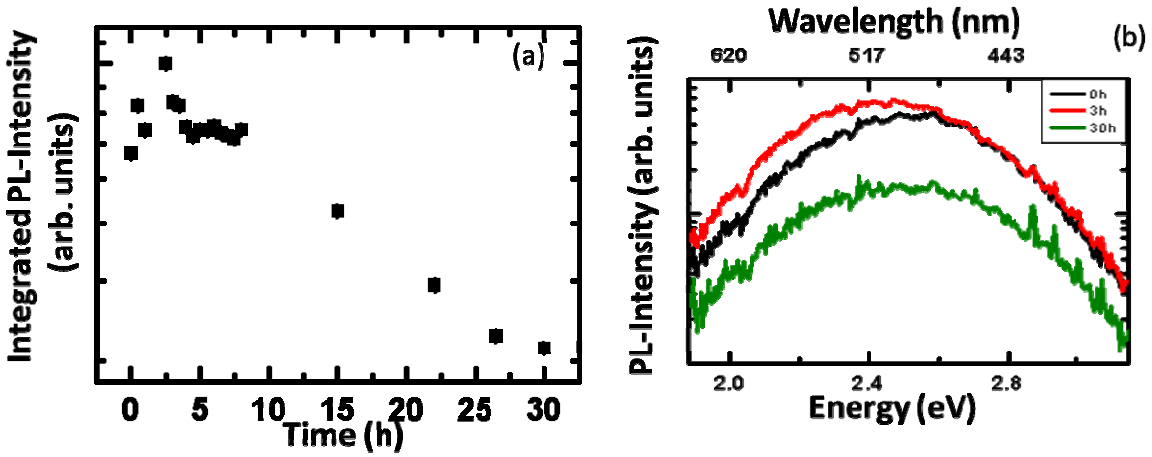

Figure 3: Integrated PL-Intensity for long-term, low density measurements (a) First spectrum, spectrum at highest integrated intensity and last spectrum (b).

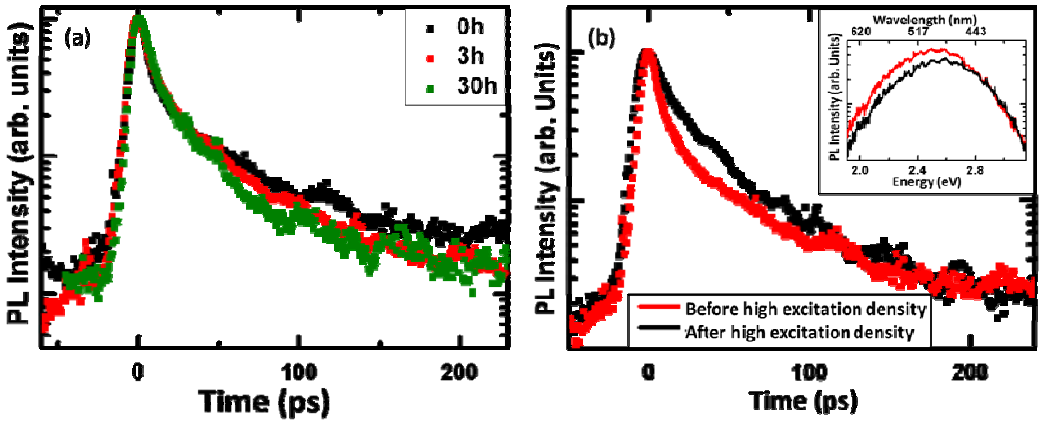

Figure 4: Time evolution of the transients for low density excitation (a).Transients before and after illumination with high excitation density (b). Corresponding spectra to the transients (inset of (b)).

Next, we studied the behavior under high excitation density. The results are shown in Fig. 4b. The transients show a slower decay after high-density illumination, while the spectra show less PL on the low energy tail of the peak. Thus, the high-density illumination has at least partially annealed the crystal, although the initial intensity could not be reached again. To increase our understanding of this behavior, further measurements in combination with x-ray diffraction (XRD) measurements are planned.

[1] E. Leusmann and S. Dehnen, Research Summary *Towards Connection of Chelating Ligands and Ruthenium Complexes to Tin/Sulfur Clusters;* annual GRK 1782 Meeting, Hofheim (2013).

Formation, Synthesis and Characterization of Binary and Ternary Functionalized Chalcogenidometallate Complexes

Jens P. Eußner, S. Dehnen

Fachbereich Chemie, Philipps-Universität Marburg

Investigations of Group 14 chalcogenidometallates have increasingly attracted attention due to potential technological applications requiring semiconducting, photoconducting, non-linear optical, catalytic or ion exchange properties.[1] Targeting of respective organic derivatives involved the development of synthetic methods for introduction of the organic ligands. In order to enhance the variety of the desired compounds, to design and combine specific physical and chemical properties by tuning the cluster moiety and storing desirable information in the components by further organic reactions, the use of functional ligands evolved to be a promising approach.[2] Particularly $[(R^1Sn)_4S_6]$ (R^1 = $CMe_2CH_2C(O)Me$) has shown to be a promising precursor towards further extension of the inorganic core and derivatizations of the complex at the organic substituents – with or without rearrangement of the cluster core.[3,4]

The dynamic behavior of chalcogenidotetrelate clusters and complexes in solution is an intrinsic feature within this chemistry and affords remarkable topologies and bonding situations.[5] The understanding of these processes represent the basis for a directed synthesis and hence the design of new tailor-made compounds of this class. For this reason the formation of functionalized tin chalcogenide complexes $[(R^1Sn)_yE_xCl_z]$ (E = S, Se, Te) was systemically investigated. For functionalized tin sulfide complexes it was shown by a combination of ^{119}Sn NMR titration experiments and DFT calculation that a stepwise condensation occurs in solution. This enabled the *a posteriori* finding of intermediates and their structural as well as spectroscopic characterization, i.e. $[(R^1SnCl_2)_2(\mu\text{-}S)]$ (**1**), $[(R^1SnCl)_2(\mu\text{-}S)_2]$ (**2**) and $[(R^1Sn)_3S_4Cl]$ (**3**). The condensation of the complexes can be controlled by the stoichiometry of the starting reagents (R^1SnCl_3 and $(SiMe_3)_2S$) and their solubility.[6] Similar behavior was found for functionalized tin selenide ($[(R^1SnCl_2)_2(\mu\text{-}Se)]$ (**4**), $[(R^1SnCl)_2(\mu\text{-}Se)_2]$ (**5**), and $[(R^1Sn)_3Se_4Cl]$ (**6**) and $[(R^1Sn)_3Se_4][SnCl_3]$ (**7**))[7] and tin telluride complexes ($[(R^1SnCl_2)_2(\mu\text{-}Te)]$ (**8**), $[(R^1SnCl)_2(\mu\text{-}Te)_2]$ (**9**), and $[(R^1Sn)_4Te_6]$ (**10**)). Especially organotin telluride complexes recently received notable attention.[8]

Derivatizations at the organic substituents of the organotin selenide complexes were performed. The reaction of **6** and **7** with hydrazine hydrate and phenyl hydrazin led to $[(R^2Sn)_3Se_4Cl]$ (**11**), $[(R^2Sn)_3Se_4][SnCl_3]$ (**12**) (R^2 = $CMe_2CH_2C(NNH_2)Me$) and $[(R^3Sn)_3Se_4][SnCl_3]$ (**13**) (R^3 = $CMe_2CH_2C(NNHPh)Me$) under retention of the inorganic core.[7] Reaction of **3** and **6** with $[Cu(PPh_3)_3Cl]$ and excess of $(SiMe_3)_2E$ led to extension of the inorganic core and generation of two ternary functional chalcogenidometallate complexes with Cu−Sn-bonds – $[C_{60}H_{74}Cl_2Cu_2O_4P_2S_8Sn_6]$ (**14**) and $[C_{72}H_{96}Cu_4O_6P_2Se_{12}Sn_7]$[7] (**15**) (Figure 1, top).

New functional groups have been successfully introduced to the organic decoration of the organotin chalcogenide complexes by a bottom-up-approach. This implied the synthesis of functional organotin trichloride compounds (R^FSnCl_3, R^F = functional organic ligand) and the consecutive reaction to functional organotin chalcogenide complexes $[(R^FSn)_xSn_yE_z]$. Until now two novel complexes were successfully synthesized – $[(\{R^4Sn\}_2SnS_4)(\mu\text{-}S)_2]$ (**16**) R^4 = $CMe_2CH_2C(O)CHCCMe_2$) and $[(R^5Sn)_4S_6]$ (**17**) (R^5 = *para*-vinylbenzene) (Figure 1, bottom). First experiments to functionalize a Si(001) surface with this complexes and modify the band structure are object of current research.

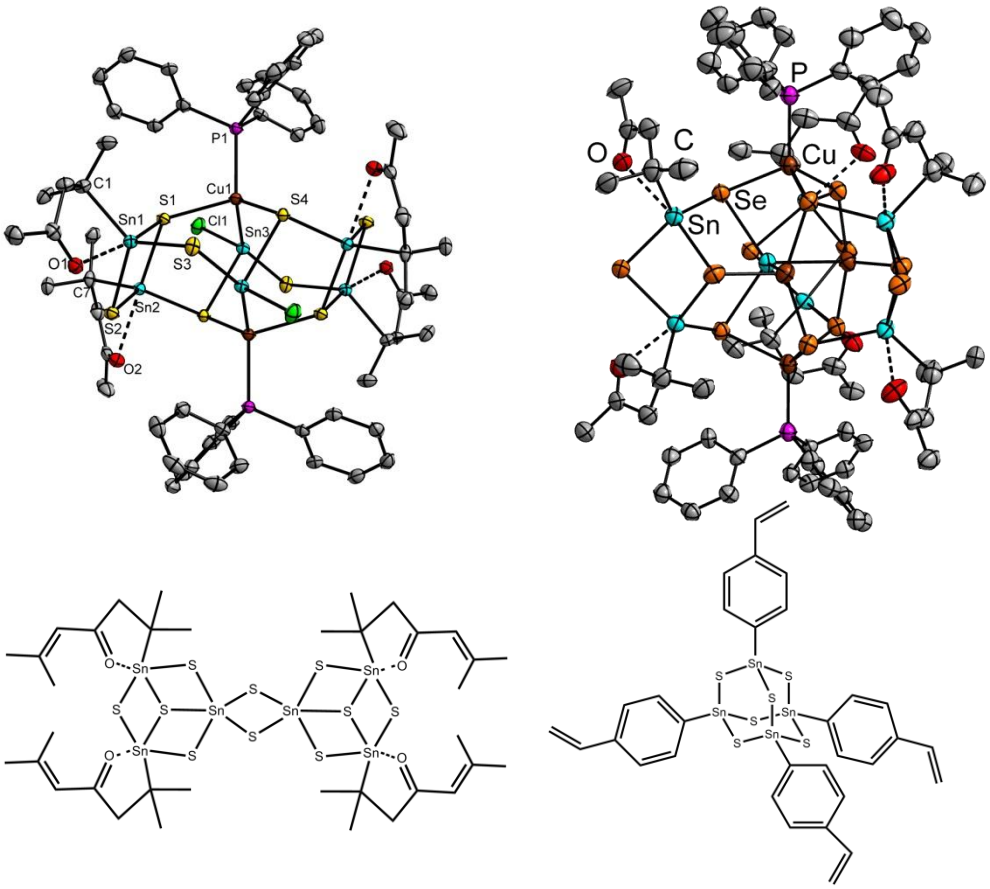

*Fig.1: (up) Crystal structures of **14** (left) at 50 % probability and **15** (right) at 30 % probability. H atoms are omitted for clarity. (bottom) Schematic figure of **17** (left) and **18** (right).*

In conclusion several new functional organotin chalcogenide complexes have been synthesized and characterized and the formation of the organotin sesquichalcogenides was systematically investigated. New organic substituents were introduced to directly functionalize the surface of semiconductors.

Future work will focus on the introduction of novel functionalities, especially with complementary reactivity towards semiconductor surfaces (i.e. alkenes, alkynes, azides). Another focus will include the reactivity and the optoelectronical properties of the already obtained complexes. The organotin chalcogenide complexes show a bathochromic shift from S, Se to Te, which will be of interest in following optoelectronical studies.

References

[1] a) R. R. Chianelli, T. A. Pecoraro, T. R. Halber, W. H. Pan, E. I. J. Stiefel, *J. Catal.* **1984**, *86*, 226–230; b) J. B. Parise, Y. Ko, J. Rijssenbeek, D. M. Nellis, K. Tan, S. Koch, *J. Chem. Soc., Chem. Commun.* **1994**, 527; c) R. L. Glitzendanner, F. L. Di Salvo, *Inorg. Chem.* **1996**, *35*, 2623–2626; d) C. L. Bowes, G. A. Ozin, *Adv. Mater.* **1996**, *8*, 13–28; e) U. Simon, F. Schüth, S. Schunk, X. Wang, F. Liebau, *Angew. Chem. Int. Ed. Engl.* **1997**, *36*, 1121–1124; f) C. R. Evenson IV, P. K. Dorhout, *Z. Anorg. Allg. Chem.* **2001**, *627*, 2178–1282; g) J. Llanos, C. Mujica, V. Sanchez, O. J. Pena, *J. Solid State Chem.* **2003**, *173*, 78; h) S. Bag, P. N. Trikalitis, P. J. Chupas, G. S. Armatas, M. G. Kanatzidis, *Science* **2007**, *317*, 490–493; i) B. D. Yuhas, A. L. Smeigh, A. P. Samuel, Y. Shim, S. Bag, A. P. Douvalis, M. R. Wasielewski, M. G. Kanatzidis, *J. Am. Chem. Soc.* **2011**, *133*, 7252–7255.

[2] a) P. Gouzerh, A. Proust, *Chem. Rev.* **1998**, *98*, 77–111; b) Z.H. Peng, *Angew. Chem. Int. Ed.* **2004**, *43*, 930–935.

[3] Z. Hassanzadeh Fard, L. Xiong, C. Müller, M. Hołyńska, S. Dehnen, *Chem. Eur. J.* **2009**, *15*, 6595-6604. b) J. P. Eußner, S. Dehnen, *Z. Anorg. Allg. Chem.* **2012**, *638*, 1827−1832.

[4] a) Z. Hassanzadeh Fard, R. Clerac, S. Dehnen, *Chem. Eur. J.* **2010**, *16*, 2050−2053; b) M. R. Halvagar, Z. H. Fard, S. Dehnen, *Chem. Commun.* **2010**, *46*, 4716-4718; c) M.R. Halvagar, Z. Hassanzadeh Fard, S. Dehnen *Inorg. Chem.* **2009**, *48*, 7373−7377.

[5] a) Z. Hassanzadeh Fard, C. Müller, T. Harmening, R. Pöttgen, S. Dehnen, *Angew. Chem. Int. Ed.* **2009**, *48*, 4441−4444; *Angew. Chem.* **2009**, *121*, 4507−4511; b) Z. Hassanzadeh Fard, M. R. Halvagar, S. Dehnen, *J. Am. Chem. Soc.* **2010**, *132*, 2845−2849.

[6] J. P. Eußner, B. E. K. Barth, E. Leusmann, Z. You, N. Rinn, S. Dehnen, *Chem. Eur. J.* **2013**, in press.

[7] Cooperation with N. Rinn, Fachbereich Chemie, Philipps-Universität Marburg.

[8] M. Bouška, L. Dostál, Z. Padělková, A. Lyčka, S. Herres-Pawlis, K. Jurkschat, R. Jambor, *Angew. Chem.* **2012**, *124*, 3535-3540; *Angew. Chem. Int. Ed.* **2012**, *51*, 3478−3482.

Towards Connection of Chelating Ligands and Ruthenium Complexes to Tin/Sulfur Clusters

Eliza Leusmann and Prof. Dr. Stefanie Dehnen*

Faculty of Chemistry and Material Sciences Center, Philipps-Universität Marburg

In recent years, the design of ruthenium complexes has attracted great interest due to their properties, which are useful for diverse applications: the utilization of Ru(II) complexes ranges from dye-sensitized solar cells[1] and chromophores[2] to water oxidation[3], for instance. Many of these complexes include chelating *N*-donor ligands like terpyridines.[1]
In our group, we have developed ligands for organotetrel-chalcogenide cages, especially a double-decker-like RSn/S cluster based on an inorganic Sn_4S_6 core, to make the organic shell reactive toward further functionalization. Starting out from a keto-functionalized ligand R = CMe_2CH_2COMe, reactions with hydrazine-derivatives have been successful (scheme 1).[4,5]

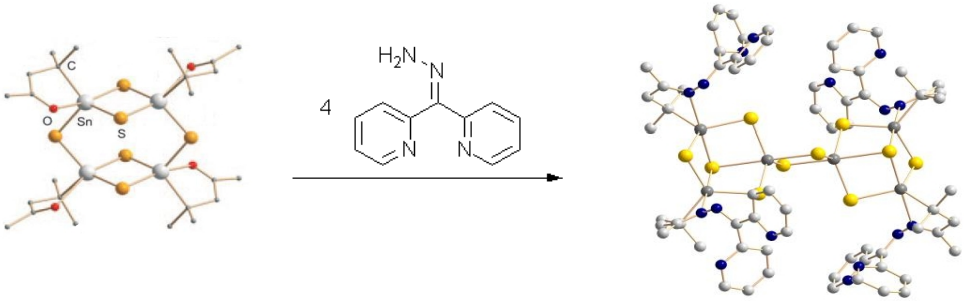

Scheme 1: Core-rearrangement and functionalization of the double-decker-like cage [$(RSn)_4S_6$] (R = CMe_2CH_2COMe) upon reaction with 2,2'-(hydrazonomethylene)dipyridine.

To combine the versatile properties of the inorganic cluster core with the potentially applicable properties of Ru(II) complexes, one of our current aims is to attach these to an Sn/S cage. This can be achieved following different ways: either by functionalization of the Sn/S cluster with a suitable donor ligand and subsequent Ru(II) sequestration, or by attachment of one of the ligands of a pre-formed Ru(II) complex to the cluster. So far, it was possible to trap Zn(II) ions by the 2,2'-(hydrazonomethylene)dipyridine-substituted cluster shown above.[5] Also the connection of acetylruthenocene to the Sn/S cluster was successful (scheme 2)[6], showing the potential of transition metal addition.

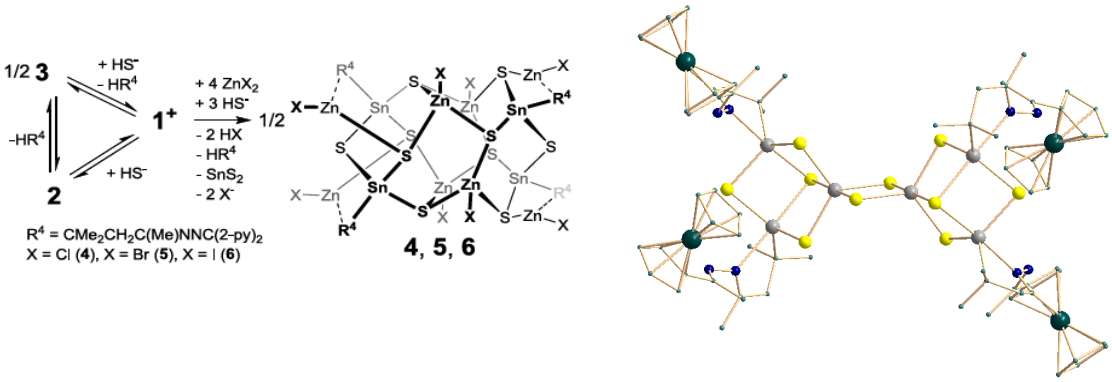

Scheme 2: Trapping of Zn(II) ions by the 2,2'-(hydrazono-methylene)dipyridine-substituted cluster[5] (left) and tethering of hydrazine-derivatized ruthenocene to the Sn/S cluster (right)[6].

In the last year, we concentrated on synthesizing organic ligands to attach them to the Sn/S cluster. The ligands are shown in scheme 3.

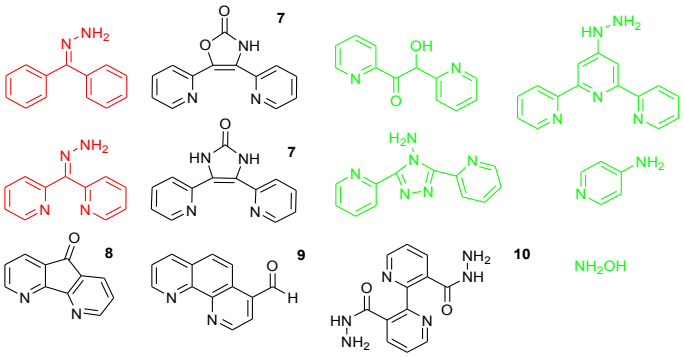

Scheme 3: Ligands synthesized for functionalization of the Sn/S cluster (green: bought ligands, red: successful attachment).

We tried either to attach the hydrazone-functionalized ligands to the ketone-cluster or to attach the ketone-functionalized ligand to the hydrazone-derivatized Sn/S cluster when it wasn't possible to synthesize a hydrazone-functionalized ligand. Only the two bipyridyl-ligands marked in red could successfully be attached to Sn/S clusters.[5] Continuative research concerned the trapping of transition metal salts or complexes (e.g. TmX_2 (Tm = transition metal, X = halogene), RuL_2Cl_2 (L = chelating ligand), $[Ru(acac)_2(CH_3CN)_2]PF_6$, $ReCl(CO)_5$) with these clusters but has not been successful so far. The main problems lie within the solubility of either the complexes and salts or the emerging compounds, which could not be crystallized yet.

Further work includes new chelating ligands and new functional groups for the connection of ligands to the cluster which should not include hydrazine derivatives. Besides, new complexes with CO-ligands should be used. Another approach is the direct attachment of a $SnCl_3$-group to a chelating ligand to gain an Sn/S cluster with a chelating moiety at the beginning, as one of our bachelor students (whom I parented) tried[11] (scheme 4).

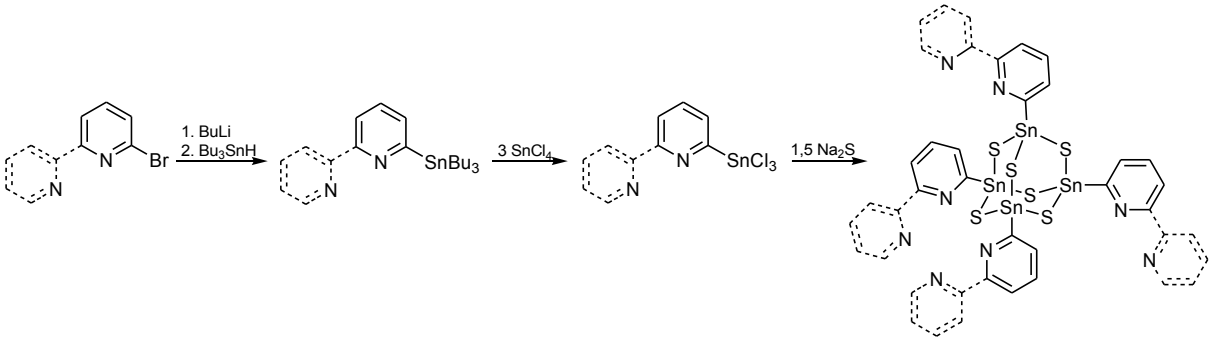

Scheme 4: Planned synthesis for an Sn/S cluster whose starting agent bears a chelating moiety.[11]

(1) P. G. Bomben, T. J. Gordon, E. Schott, C. P. Berlinguette, Angew. Chem. **2011**, 123, 10870-10873. (2) K. C. D. Robson, C. P. Berlinguette et al., Inorg. Chem. **2011**, 50, 5494-5508. (3) B. Radaram, X. Zhao et al., Inorg. Chem. **2011**, 50, 10564-10571. (4) Z. Hassanzadeh Fard, L. Xiong, C. Müller, M. Hołyńska, S. Dehnen, Chem. Eur. J. **2009**, 15, 6595-6604. (5) B. E. K. Barth, E. Leusmann, K. Harms, S. Dehnen, *Chem. Commun.* **2013**, *49*, 6590-6592. (6) E. Leusmann, M. Wagner, S. Dehnen, *in preparation*. (7) D. Blum, *Chem. Ber.* **1956**, *90*, 391. (8) M. J. Plater, S. Kemp, E. Lattmann, *J. Chem. Soc., Perkin Trans.1*, **2000**, 971-979. (9) S. H. Bossmann, N. J. Turro *et al.*, *Synthesis* **1996**, *11*, 1313. (10) S. Dholakia, F. L. Wimmer *et al.*, *Polyhedron* **1985**, *4*, 791; C.-Z. Zhang, J.-C. Tao *et al.*, *Inorg. Chim. Acta* **2007**, *360*, 448-454. (11) Florian-David Lange, *Bachelor Thesis*, Marburg **2013**.

Ternary Intermetalloid Clusters and Zintl Anions: Reactions of Binary Zintl Anions with Lanthanide Complexes

Bastian Weinert, Prof. Dr. Stefanie Dehnen

Department of Chemistry and Material Sciences Center, Philipps-Universität Marburg

Introduction

Intermetalloid clusters,[1] which combine main group (semi-)metals with transition metal clusters, belong to the most recent developments in the field of *Zintl* anion chemistry and physics.[2] So far, the clusters have usually been obtained by reacting solutions of *Zintl* phases A_4Tt_9 or A_3Pn_7 (A: alkali metal, Tt: tetrel, Pn: pnictogen), which comprise homoatomic anions, in liquid NH_3 or *en*/[2.2.2]crypt with transition metal compounds.

However, due to a relatively high charge, most of the phases with molecular tetrel polyanions, e.g. A_4Tt_4, show poor solubility,[3] which has complicated reactions of further species. To overcome this problem, and to add another degree of freedom regarding the electron number of the resulting clusters, we recently extended this approach by using binary *Zintl* anions with a combination of Group 14/15 elements as well-soluble precursors, namely $[Sn_2Sb_2]^{2-}$, $[Sn_2Bi_2]^{2-}$, with only 2− charge according to the *Zintl-Klemm-Busmann*[4] pseudo element concept. This has led to the generation of a large variety of ternary anions such as $[Pd_3@Sn_8Bi_6]^{4-}$, $[Ln@Sn_7Bi_7]^{4-}$ and $[Ln@Sn_4Bi_9]^{4-}$ (Ln = La, Ce).[5,6]

Results

Our current investigations again extent this field by transferring our approach to the employment of *pseudo*-homoatomic precursors and to the Group 13/15 element combination $[GaBi_3]^{2-}$ and $[InBi_3]^{2-}$.[7] Here, we present first results (fig. 1) of this variation that indicate the subtle influence of charges, atomic radii and Lewis basicities of the involved elements.

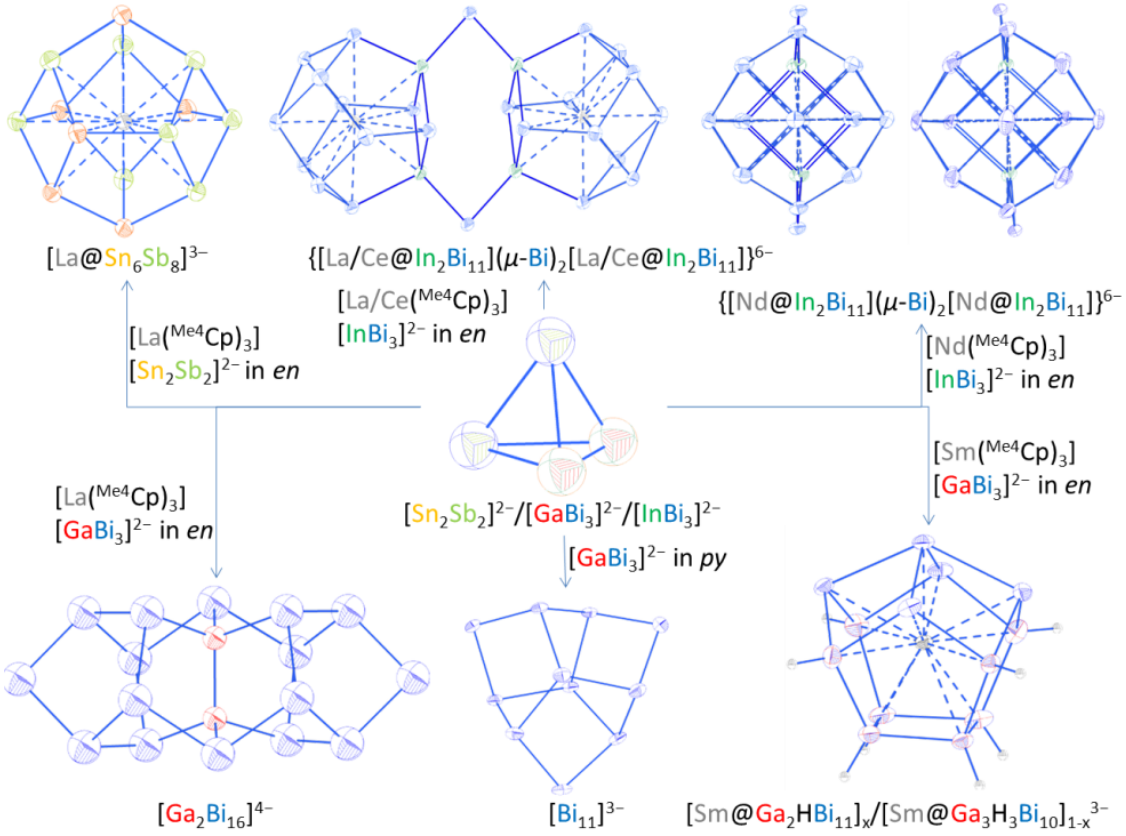

Fig.1: Reaction scheme with resulting intermetalloid clusters and Zintl anions.

We obtained clusters with novel structures or different charges, $\{[La/Ce/Nd@In_2Bi_{11}](\mu\text{-}Bi)_2[La/Ce/Nd@In_2Bi_{11}]\}^{6-}$ or $[La@Sn_6Sb_8]^{3-}$.[8,9] We were able to first synthesize protonated intermetalloid clusters $[Sm@Ga_2HBi_{11}]_x/[Sm@Ga_3H_3Bi_{10}]_{1-x}^{3-}$,[9] which brings us closer to uncharged and therefore even better soluble species. Furthermore we could achieve bismuth rich polyanions, that were unknown to date – such as $[Bi_{11}]^{3-}$ and $[Ga_2Bi_{16}]^{4-}$.[9] Besides characterization of the compounds, our studies include formation mechanisms and electronic structures of the uncommon intermetalloid cages and their complex behavior in solution.

Conclusions

We performed ^{71}Ga, ^{1}H, ^{13}C, HSQC and HMBC nuclear magnetic resonance, mass spectrometry, infrared spectrum and quantum chemical investigations. We can now explain the function of the lanthanide precursor ligands, which had been unclear for a long time.

Additionally, we could prove our concept of using binary Zintl anions for being a proper approach in generating new intermetalloid clusters and widen the field by use of Group 13/15 anions. Even long missed anions are now available via our method.

Outlook: what ist planned

We are interested in crystallizing our binary and ternary anions onto semiconductor surfaces via crystallization from solution or via gas phase anion deposition in an electric field.

Furthermore we are planning to selectively decompose our compounds generating binary, ternary or quarternary phases and prove their application as heterogeneous catalysts.

References

[1] T. F. Fässler, S. D. Hoffmann, *Angew. Chem. Int. Ed.* **2004**, *43*, 6242;
[2] S. Scharfe, F. Kraus, S. Stegmaier, A. Schier, T. F. Fässler *Angew. Chem. Int. Ed.* **2011**, *50*, 3630;
[3] M. Waibel, F. Kraus, S. Scharfe, B. Wahl, T. F. Fässler, *Angew. Chem. Int. Ed.* **2010**, *49*, 6611;
[4] W. Klemm, E. Busmann, *Z. Anorg. Allg. Chem.* **1963**, *319*, 297;
[5] F. Lips, R. Clérac, S. Dehnen, *J. Am. Chem. Soc.* **2011**, *133*, 14168;
[6] F. Lips, M. Hołyńska, R. Clerac, U. Linne, I. Schellenberg, R. Pöttgen, F.Weigend, S. Dehnen, *J. Am. Chem. Soc.* **2012**, *134*, 1181;
[7] L. Xu, S. C. Sevov, *Inorg. Chem.* **2000**, *39*, 5383;
[8] B. Weinert, F. Weigend, S. Dehnen,* *Chem. Eur. J.* **2012**, *18*, 13589–13595;
[9] in preperation.

Optical Spectroscopy on Planar Organic/Inorganic Hybrids

I. Meyenburg, T. Breuer, G. Witte and W. Heimbrodt

Fachbereich Physik, Philipps Universität Marburg, Renthof 5, 35032 Marburg

Introduction

Organic - inorganic semiconductor hybrid systems combine the optoelectronic variability of organic materials with a high carrier mobility of the anorganic semiconductor. The resulting hybrid systems have attracted a lot of attention due to their versatile electronic properties and low temperature processing. It has been shown, for example, that inorganic organic hybrids like p-type Pentacene ($C_{22}H_{14}$) on optical transparent n-conductive ZnO are feasible to prepare p-n-junction. Pentacene has a high carrier mobility (3cm /V s). So it is one of the most promising organic semiconductors for electronic devices.

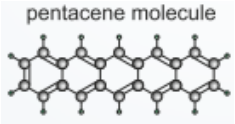

We used optical spectroscopy to analyze the optical, electronic and vibrational properties of hybrid samples which were prepared in the group of Prof. Witte.

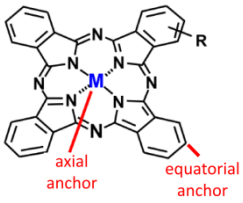

Copper-Phthalocyanine (CuPc), which is a promising organic material for an all solid-state dye sensitized solar cell, was investigated on different substrates (Glass, KCl, NaCl) and in solution. First results are shown here. CuPc will be investigated intensively in a hybrid system in future. A fast electron transfer from the dye into the inorganic semiconductor is important for a good device efficiency. For a fast electron transfer the band alignment at the interface is crucial. It can be influenced by variation of the Phthalocyanine by different anchor groups. Optical measurements enable to investigate the band parameter when connected with an inorganic substrate (e.g. TiO_2).

Results

In order to study the excitonic properties of the organic layer we prepared pentacene films on ZnO surfaces by molecular beam deposition under ultra-high vacuum (details see [1]).

By varying the growth temperature during deposition we obtain different pentacene films. While at 136K a poly-crystalline layer builds up the thin crystalline thin film phase is grown at room temperature. At 353K the Campbell phase evolves. In comparison to the penta-cene molecules in solution the absorption spectra of the crystalline pentacene exhibit additional pro-nounced Davydov-splitted excitonic features due to the interaction of two mole-cules in the unit-cell.

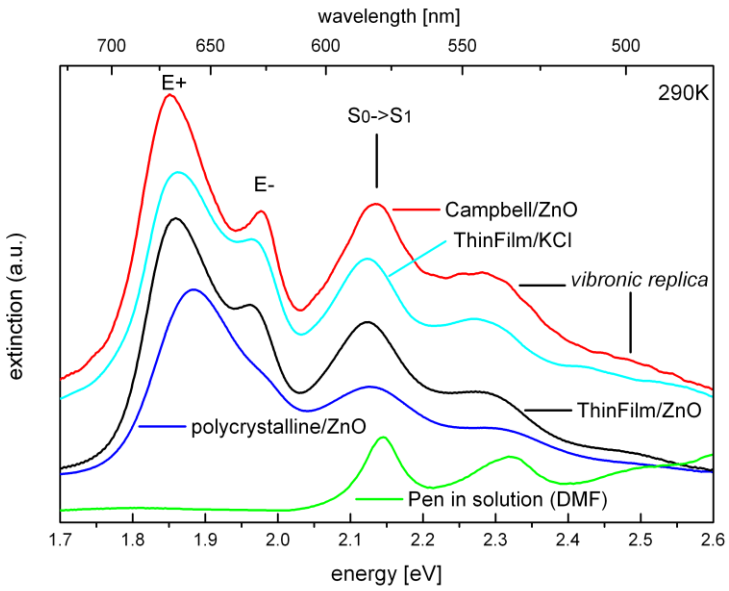

Fig.1: Extinction of Pentacene
Pentacene in solution shows no exitonic features in contrast to Campbell and ThinFilm phase deposited on ZnO and KCl

Photoluminescence measurements were done at different excitation energies (Laser wavelength 325nm, 442nm and 532nm) for Pentacene samples.

Early results showed a temperature dependence of the two exciton absorption bands for different thicknesses.[1] This is due to the very different thermal expansion coefficients of Pentacene and ZnO. So the adlayer of the film is under substantial strain whereas the successive monolayers can relax step by step. The strain leads to a decrease of the exciton binding energy and an increase of absolute absorption energy. Strain effects of different substrates could also be shown, the strain is lower for substrates with thermal coefficients which are closer to the one of pentacene.
The Davydov splitted excitonic features of Thin Film Pentacene on ZnO have dipole moments perpendicular to each other which show characteristic polarization dependence. Further absorption measurements were done which reveal the temperature dependence of the features. The Herringbone angle between the two molecules of the unit cell can be calculated from the unpolarized absorption measurement. The angle decreases with decreasing Temperature, especially for the Campbell phase (293K:50° → 10K:33°).

First layers of CuPc were successfully prepared with orientation either parallel to the substrate plane (NaCl) or normal to the substrate (glass) (Fig.3). Also CuPc solved in DiClBenzene is shown.

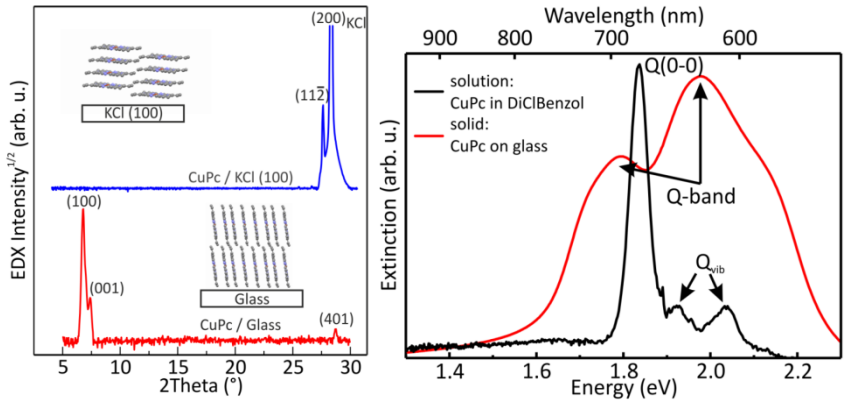

*Fig.3: Left: XRD measurements show the flat alignment of CuPc on KCl and the upright alignment on glass.(Group Witte) Right: The Q-bands (π to π * transitions) of the films are broadened compared to the molecules in solution due to the weak intermolecular coupling (van der Waals interaction).*

Conclusions

The strain between ZnO substrate and Pentacene layer leads to tremendous shifts of the exciton states and the $S_0 \rightarrow S_1$ bandgap in dependence of the temperature. The herringbone angle especially for Campbell phase also varies with temperature. We found very interesting preliminary results on CuPc. A strong broadening occurs of the molecular Q-states due to the band formation. The CuPc layers exhibits a pronounced anisotropy which could be measured in absoption as well as photoluminescence in dependence on the orientation of the crystalline films.

Outlook

Very smooth ZnO substrates will be used to prepare hybrids in even better quality and bigger crystallite size. We will analyze the polarization dependence of the absorption of a single crystallite. Cu-Phthalocyanine (also with modified anchors) in solution and on different substrates including transparent conductive oxides will be investigated by means of absorption, photoluminescence and time resolved photoluminescence spectroscopy. The electron phonon interaction and possible excitonic effects will be examined.

[1] M. El Helou, E. Lietke, J. Helzel, W. Heimbrodt and G. Witte, J. Phys.:Condens. Matter **24,** 445012 (2012)

Multiplexed Measurements by Time Resolved Spectroscopy using Colloidal CdSe/Zns Quantum Dots

U. Kaiser, R. Malinowski, D. Jimenez de Aberasturi, W. J. Parak, and W. Heimbrodt

Fachbereich Physik, Philipps Universität Marburg, Renthof 5, 35032 Marburg

Introduction

Quantitative analysis of different analytes in a solution simultaneously is a very demanding topic for bio analytic applications. There is still a strong restriction of so called multiplexed sensing with optical methods. Due to the broad luminescence bands of the used dye sensor molecules there is a limitation to simultaneously detection to only a few molecules at a time. With time dependent measurements of the dye molecules photoluminescence (PL) we want to overcome this obstacle. The basic idea is, to use two dye sensors with the same spectral information, but with significant different time behavior of the PL. To obtain these different time characteristics we want to use functionalized semiconductor quantum dots, because of their access to the whole visible spectrum by size variation and high quantum yield. By the quantitative analysis of the PL transients we are then capable to determine the exact concentration of both dye sensor molecules.

Results

For our initial investigations we started with two model systems. On the one hand we synthesized gold nanoparticles (AuNPs) with an amphiphilic polymer shell. In the polymer shell of these AuNPs we embedded dye molecules (ATTO-590) with a luminescence maximum at 620 nm. To create our modified dye sensor we coupled the same molecules to the polymer shell of colloidal CdSe/ZnS quantum dots (QDs), yielding a luminescence maximum at the same spectral position as the ones bound to the AuNPs. We did time resolved measurements with a 10 Hz pulsed Nd:YAG laser operating at a wavelength of 355 nm. The samples were investigated in aqueous solution at room temperature. In Fig. 1 the transients of the individual samples are depicted, dye bound to AuNPs, CdSe/ZnS QDs and dye bound to the QDs. The dye molecules bound to the AuNPs show a mono-exponential decay behavior with a decay constant of 4.5 ns (red circles) in Fig. 1. The PL of the semiconductor QDs (black squares) on the other hand shows a typical bi-exponential decay with a long lifetime of 134 ns. The decay characteristics of the QDs are determined by a radiative transition and an energetically lower trap state.[1] The dye molecules bound to the CdSe/ZnS QDs (blue triangles) on the other hand exhibit a decay behavior which is determined by the radiative lifetime of the dye and the decay characteristics of the QD. This is due to the energy transfer from the QD to the dye molecules coupled to the shell of the CdSe/ZnS dot. The rate equation for the dye bound to the QDs can be solved with a triple exponential function. The

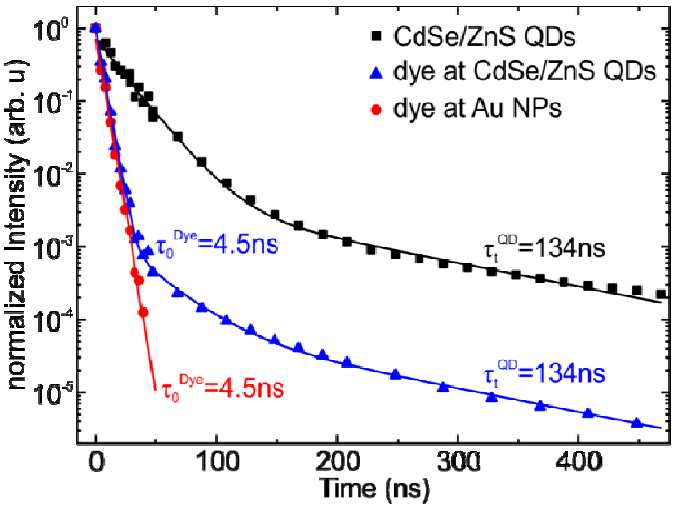

Fig.1: Measured PL decay for the CdSe/ZnS quantum dots, dye bound to AuNPs, and dye bound to CdSe/ZnS QDs with respective fitting curves.

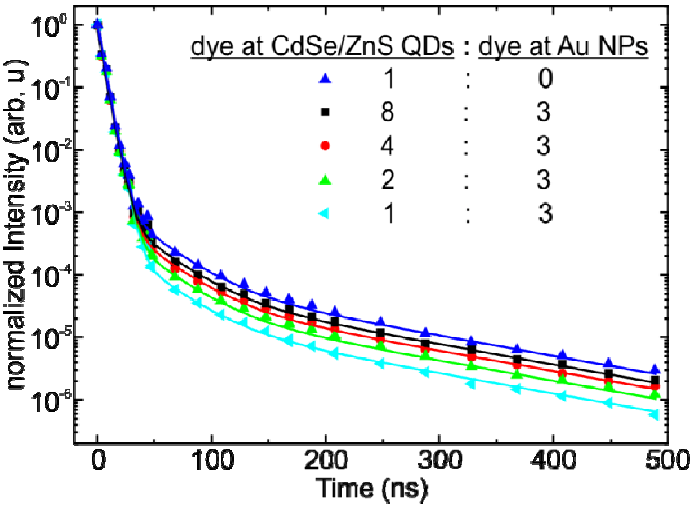

Fig.2: PL decay for different mixing ratios of the fast dye (bound to Au NPs) and the slow dye (bound to CdSe/ZnS QDs) with respective fitting curves.

fit hereby yields similar time constants as the ones obtained from the dot and the dye bound to AuNPs. The solid lines in Fig. 1 represent the fitting curves belonging to the mono-, bi- and triple-exponential PL decay of the dye coupled to AuNPs, the QDs and the dye bound to QDs, respectively. With the size control of the QDs we were able to tune the energy transfer from the dot to the bound dye in the exact manner we needed, due to the changed spectral overlap for different dot sizes.[2] As can be seen in Fig. 1 we obtain a fast dye molecule (bound to AuNPs) and a slow one (bound to CdSe/ZnS QDs). To distinguish between these two dyes in a single solution one has to be able to determine the concentrations of both dyes for a given sample. In Fig. 2 the transients for different mixing ratios of both dyes are depicted. As one can see there is a faster decay for higher concentrations of the dye bound to AuNPs, which is the so called fast dye. The solid lines represent the triple exponential fitting curves, with the same constants used above. For the fitting of the data in Fig. 2 we used only one free parameter which is related to the ratio of both dye molecules in a given solution.

Conclusion

We could show that we are able to create a dye sensor with a tremendously increased lifetime, by coupling it to a semiconductor QD. We were also able to distinguish between this ´new slow dye´ and the same dye with a fast decay behavior in a single solution. The fitting curves for a given mixing ratio of both dyes lie in perfect agreement to the measured data, which allows for a very accurate determination of the mixing ratio.

Outlook

For future applications we want to extend this method to ion sensitive dye molecules. Therefore we want to couple different ion sensitive dye molecules in the same spectral range to CdSe/ZnS QDs and AuNPs respectively. With the time resolved measurements we will then be able to detect different ion concentrations simultaneously in a given solution.

[1] A. Efros. M. Rosen, M. Kuno, M. Nirmal, D. Norris, and M. Bawendi, Physical Review B **54**, 4843 (1996)
[2] T. Niebling, F. Zhang, Z. Ali, W. J. Parak, and W. Heimbrodt, Journal of Applied Physics **106**, 104701 (2009)

Adsorption of Tetrahydrofuran on the Si(001) surface studied by means of STM, XPS and UPS

M. Reutzel[1], G. Mette[1], U. Koert[2], M. Dürr[1,3], and U. Höfer[1]

[1] *Fachbereich Physik und Zentrum für Materialwissenschaften, Philipps-Universität, D-35032 Marburg, Germany*
[2] *Fachbereich Chemie, Philipps-Universität, D-35032 Marburg, Germany*
[3] *Institut für Angewandte Physik, Justus-Liebig-Universität Giessen, D-35392 Giessen, Germany*

1. Introduction

A promising possibility to compete with the challenges of miniaturization in semiconductor device physics is the functionalization of inorganic semiconductor surfaces with organic molecules [1]. In this context, it is important to understand the basic adsorption mechanisms, adsorption dynamics, and surface reactions. Within the work of the GRK 1782 we aim to investigate the interaction of the often used organic solvent tetrahydrofuran (THF) with the Si(001) surface. Within the first year in the GRK, we have studied the adsorption geometry of THF on Si(001) by means of XPS and UPS [2].

2. Results

The STM-images of Fig. 1 show the adsorption of THF on Si(001) [3]. At room temperature, Fig. 1 (a) indicates an adsorption geometry across two dimer rows. The bright spots are located over the outer dimer atoms and are interpreted as dangling-bond configurations. Accordingly, the dark centers are attributed to the THF molecule. At 50 K, a completely different adsorption geometry is observed (Fig 1 (b)). Comparing the adsorption sites with the zick-zack structure of the Si(001) c(4 × 2) surface, a site selective adsorption over the lower dimer atom is observable. The low temperature phase transfers irreversibly into the room temperature phase.

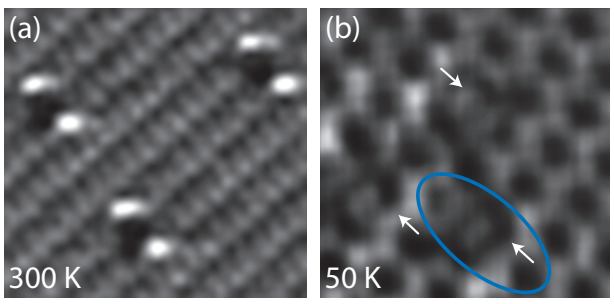

Figure 1: (a) STM-image (6×6 nm^2) of Si(001) after the adsorption of 0.02 ML THF at T_S = 300 K at positive sample bias (+0.8 V, 0.5 nA). (b) STM-image (6×6 nm^2) of Si(001) after the adsorption of 0.02 ML THF at T_S = 50 K at positive sample bias (+0.8 V, 0.3 nA) [3].

For the identification of the observed adsorption geometries, X-ray photoelectron spectroscopy (XPS) was performed. Fig. 2 (a) and (b) show the O1s and C1s spectra of $\leq$ 1 ML THF on Si(001), respectively. The O1s spectra indicate a phase transition from the LT phase ($E_{\mathrm{B}}^{LT} = 535.0$ eV, blue) to the RT phase ($E_{\mathrm{B}}^{RT} = 532.2$ eV, red) by an energetic shift of $\Delta E_{\mathrm{B}}^{LT-RT} = 2.8$ eV to lower binding energies. At 50 K, the symmetric α-**C** : β-**C** = C-**C**-C : C-**C**-Si lines in the C1s spectra are attributed to an intact molecule (intensity ratio 1 : 0.9). The O1s binding energy of a multilayer THF is $E_{\mathrm{B}}^{>1\mathrm{ML}} = 534.4$ eV (not shown). The difference in the binding energy of the multilayer and the monolayer reveals a lower valence electron density at the oxygen atom in the monolayer. In combination with the site-selective adsorption of the THF molecule at low-temperature [Fig. 1], an electron donation into the empty $\mathrm{D_{down}}$ orbital, i.e. a dative bonding situation, can be concluded.

At room-temperature, the shifted binding energy of the O1s line is attributed to a covalently attached oxygen atom to the Si(001) surface [4]. The C1s spectra does not reveal a symmetric intensity ratio anymore. In a simple approach, the chemical shift of X-ray photoemission features is dominated by neighboring atoms and their electronegativity χ. Comparing the electronegativity of the elements under inspection with $\chi_{\mathrm{O}} > \chi_{\mathrm{C}} > \chi_{\mathrm{Si}}$, the photoemission structures are attributed to C-**C**-O, C-**C**-C and C-**C**-Si, respectively. With a covalently attached oxygen atom a C-O bond cleavage and thereby a ring opening reaction seems obvious. In addition with the intensity ratio C-**C**-O : C-**C**-C : C-**C**-Si = 1 : 1.9 : 0.8 a Si-O-C-C-C-C-Si adsorption geometry is concluded.

Even more detailed information on the dative bonding situation on an orbital level is obtained by Ultraviolet photoelectron spectroscopy (UPS) [Fig. 3 (c)]. The energy scale is calibrated by the He-II spectrum of the clean Si(001) surface which shows a clearly resolved signal of the $\mathrm{D_{up}}$ orbital [5, 6]. The multilayer spectrum is comparable to the gas phase spectrum of THF, indicating an intact molecule [7]. Especially, the HOMO at $E_{\mathrm{B}}^{multilayer} = 5.8$ eV is attributed to a lone pair of the oxygen atom [7]. Interestingly, the UP spectra of the monolayer at 50 K equals the multilayer, except for the missing HOMO. The absent electron density indicates a

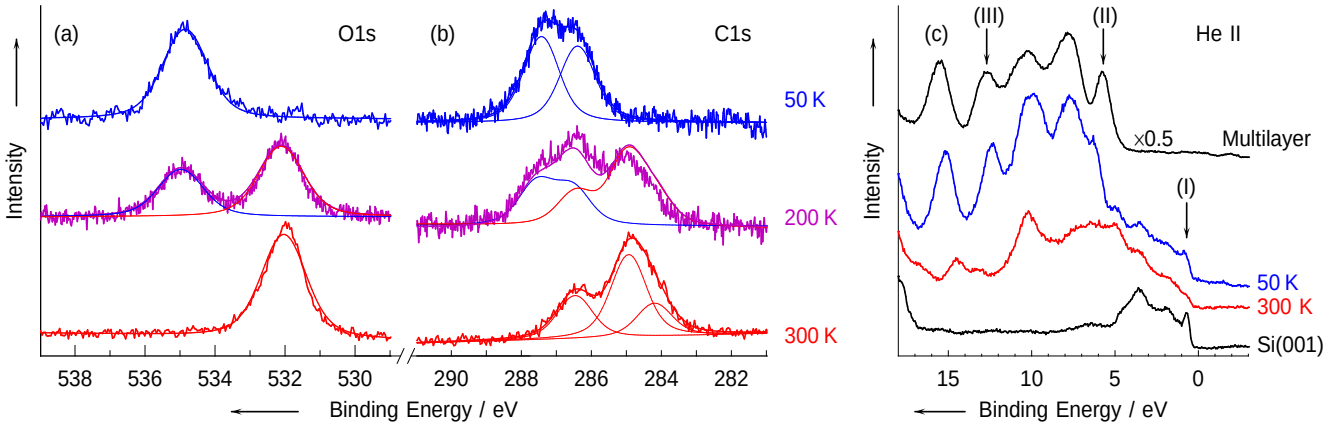

Figure 2: XP and UP spectra of THF/Si(001). (a) and (b): Peak fitted photoemission spectra of the O1s and C1s electrons of a submonolayer of THF on Si(001), respectively. (c) UP spectra of a multilayer THF adsorbed at 50 K (black line, top), a monolayer of THF on Si(001) at 50 K (blue) and 300 K (red), as well as from a clean Si(001) surface (black, bottom). The arrows in (c) indicate the occupied dangling bond surface state D_{up} (I), the HOMO of THF (II) and a delocalized molecular orbital of the THF molecule (III).

reaction of the lone pair. On the other hand, the UP spectrum is completely different at 300 K, some well defined peaks of the mulilayer spectrum have disappeared [Fig. 2 (c)]. The arrow (III) highlights the binding energy of a molecular orbital with a delocalized character over the circular THF molecule. The absent electron density at room-temperature then indicates a ring opening reaction.

3. Conclusions

Our investigations clearly identify the reaction pathway of THF with Si(001) via a dative bonding situation [Fig. 3 (b)] to a Si-O-C-C-C-C-Si adsorption geometry bridging two Si-atoms of different dimer rows [Fig. 3 (c)]. The essential ring-opening due to a C-O-bond cleavage is induced thermally and can be seen in analogy to an ether cleavage as observed organic chemistry. As far as we know, a datively bonded species involving an oxygen atom as electron donor has not been observed experimentally on Si(001) so far.

4. Outlook

Based on our results on the adsorption mechanism of THF on the Si(001) surface, we would like to expand our experiments to the functional group of ethers in more general. In a next step, we will thus investigate the adsorption of diethylether on Si(001). Furthermore it seems interesting to investigate the reaction pathway from the dative bonding situation to the room temperature configuration in more detail. Mette showed that it is possible to induce the ether cleavage not only thermally but also electronically by tip induced effects [3]. In this case, more than one adsorption configuration was observed after the ring opening reaction. To investigate the differences between the thermally and electronically activated process, a ns heating experiment will be performed which might freeze

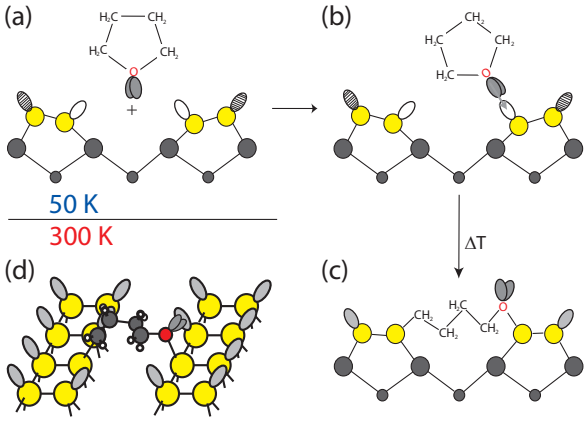

Figure 3: Schematic drawing (side view) of (a) the THF molecule above the Si(001) surface, (b) a dative bonding between the THF molecule and the Si(001) surface, and (c) the RT configuration of THF reacted on Si(001). Grey and yellow balls indicate Si atoms, the Si dangling bond states are drawn white (empty), shaded (filled), or grey (half filled). The electron lone pairs of the oxygen atoms are drawn dark grey. In (d), the latter configuration of (c) is sketched in a pseudo-3D ball-and-stick model.

out further intermediates also in the case of the thermally activated reaction [8].

[1] J. T. Yates, Science **279**, 335 (1998).
[2] G. Mette, M. Reutzel, U. Koert, M. Dürr, and U. Höfer, to be published (2013).
[3] G. Mette, Dissertation, Philipps-Universität Marburg, 2012.
[4] H. N. Hwang, J. Y. Baik, K. S. An, S. S. Lee, Y. S. Kim, C. C. Hwang, and B. S. Kim, J. Phys. Chem. B **108**, 8379 (2004).
[5] F. J. Himpsel and D. E. Eastman, J. Vac. Sci. Technol. **16**, 1297 (1979).
[6] G. V. Hansson and R. I. G. Uhrberg, Surf. Sci. Rep. **9**, 197 (1988).
[7] K. Kimura, *Handbook of Hel Photoelectron Spectra of Fundamental Organic Molecules: Ionozation Energies, Abb Inito Assignments, and Valence Electronic Structure for 200 Molecules* (Japan Scientific Societies Press, Tokio, 1981), Vol. 1.
[8] M. Dürr, A. Biedermann, Z. Hu, U. Höfer, and T. F. Heinz, Science **296**, 1838 (2002).

Adsorption dynamics of tetrahydrofuran on Si(001) studied by means of molecular beam techniques

M. Lipponer[1], M. Dürr[1;2], and U. Höfer[1]

[1]*Fachbereich Physik und Zentrum für Materialwissenschaften, Philipps-Universität, D-35032 Marburg, Germany*
[2]*Institut für Angewandte Physik, Justus-Liebig-Universität Giessen, D-35392 Giessen, Germany*

1. Introduction

The functionalization of semiconductor surfaces is one possibility to overcome the limits of conventional semiconductor devices [1]. Therefore, it is of great importance to work towards a better understanding of the basic adsorption processes and dynamics of organic molecules on silicon surfaces. Within the work of the GRK 1782 we performed molecular beam experiments of tetrahydrofuran (THF) on Si(001). Molecular beam experiments give insight on the adsorption dynamics, e.g. by measuring the dependence of the sticking propability on the kinetic energy E_{kin} of the impinging molecules or the surface temperature T_s. The results allow conclusions on the nature of the adsorption pathway and the involved energy barriers of the Lennard-Jones potential.

2. Results

To measure sticking coefficients, the King and Wells method was used in this experiment. In short, the prepared clean sample is placed in front of a quadrupole mass spectrometer (QMS) which records the background pressure of THF in the vacuum chamber as a function of time. When allowing the molecular beam into the sample chamber, the molecular beam is blocked at first, so it cannot hit the sample surface. When opening the shutter, the surface is exposed to the molecular beam and a drop in the background pressure is observed. This pressure drop is due to adsorption on the reactive surface. If the sample is larger than the molecular beam, the observed pressure drop is proportional to the initial sticking coefficient s_0.

In Figure 1, the initial sticking coefficients s_0 of THF is shown as a function of kinetic beam energy E_{kin} for three different surface temperatures T_s. For all three temperatures, s_0 decreases with increasing kinetic energy. This is typically associated with a non-activated adsorption pathway. For successful trapping of the incoming molecules, sufficient energy dissipation is required and therefore trapping becomes more unlikely the more energy the impinging molecules carry [2].

In contrast to more simple molecules such as ethylene [3], the initial sticking coefficient s_0 of THF shows a rather weak dependence on kinetic energy. This could be explained by the fact that the more complex molecular structure of THF allows for a better energy dissipation even at higher kinetic energies. The existence of additional reaction channels might furthermore contribute at higher energies.

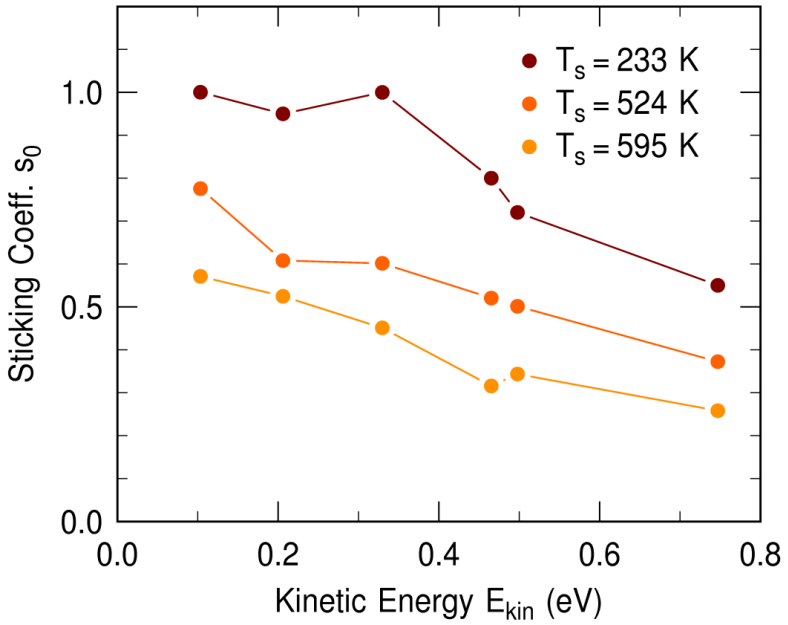

Figure 1: Initial sticking coefficient s_0 of THF on Si(001) as a function of beam energy E_{kin} at different surface temperatures T_s.

The initial sticking coefficients s_0 as a function of T_s are shown in Figure 2. It is obvious that the initial sticking coefficients remain at the same high level until a surface temperature of about 400 K. For higher temperatures s_0 drops and approaches zero. This behavior can be explained with the Kisliuk-precursor model:

Once trapped into the precursor state, molecules can either convert into the final state with a rate k_a, or desorb back into the vacuum with rate k_d. In both cases a barrier ε has to be overcome. The rates of these competing processes govern the overall temperature dependence of the sticking coefficient $s_0(T_s)$.

The dashed line in Fig. 2 represents the functional form of the sticking coefficient $s(T_s)$ according to the Kisliukmodel:

$$s_0 = s_p \cdot \left[1 + \frac{\nu_a}{\nu_d} \cdot \exp\left(-\frac{\varepsilon_d - \varepsilon_a}{k_B T_s}\right)\right]^{-1}$$

Here, ε_d-ε_a describes the difference in the barrier height within the precursor mediated adsorption pathway which has been evaluated with this data (ε_d-ε_a = 0.34 eV).

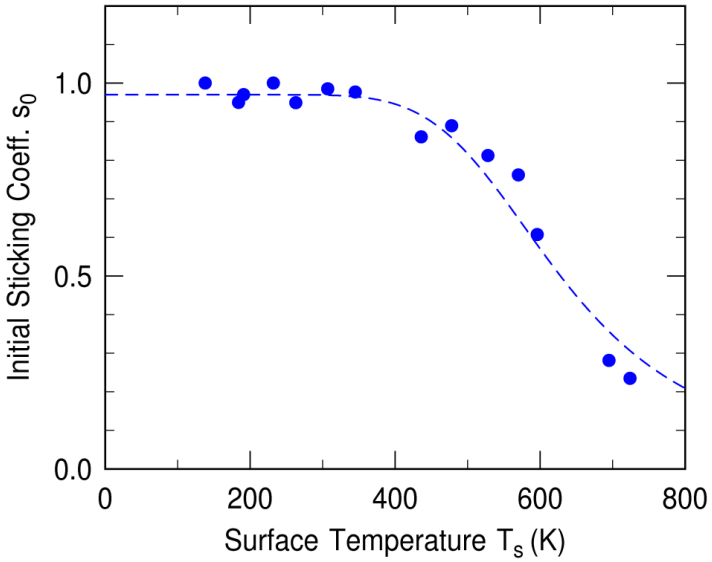

Figure 2: Initial sticking coefficient s_0 as a function of surface temperature T_s for a low beam energy. The dashed line represents the initial sticking coefficient as calculated via the Kisliuk precursor model (see Eq.1).

It becomes apparent that the Kisliuk-model and the data show very good agreement.

For comparison, the difference in barrier height for ethylene on Si(001) is smaller [3], which results in a drop of the sticking coefficient $s_0(T_s)$ at lower surface temperatures. This is an indicator for an overall stronger bond of the precursor state in the case of THF.

3. Conclusions

The molecular beam experiments we performed gave insight on the dynamics of the THF/Si(001) surface reaction. We found, that the adsorption occurs via a non-activated adsorption pathway and via an intermediate "precursor" state. The smaller energy dependence of the initial sticking coefficient s_0 implies a better energy dissipation of the impinging THF-molecules compared to smaller molecules like ethylene. The discussed precursor state is more strongly bound than, e.g., ethylene which is also supported by STM- and XPS investigations performed in our group [4]. They identified the precursor state as a "dative" bonding.

4. Outlook

In the future, adsorption dynamics of other organic molecules such as trimethylamine (TMA) will be investigated.

The reaction between TMA and the Si(001) surface is an excellent example for a Lewis acid-base reaction [5], similar to the one of THF on Si(001). We aim to investigate the adsorption pathway of the intact TMA-molecule as well as the creation of the dissociated species by means of second harmonic generation (SHG), Auger-electron spectroscopy (AES), and the King and Wells-method.

[1] J. T. Yates, Science 279, 335 (1998).
[2] A. Gross, Surf. Sci. Rep. 32, 291 (1998).
[3] M. A. Lipponer, N. Armbrust, M. Dürr, and U. Höfer, J. Chem. Phys. 136, 144703 (2012).
[4] G. Mette, M. Reutzel, U. Koert, M. Dürr, and U. Höfer, to be published (2013).
[5] M. Z. Hossain, S. Machida, M. Nagao, Y. Yamashita, K. Mukai, and J. Yoshinobu, J. Phys. Chem. B 108, 4737 (2004).

Preliminary studies for pump-probe measurements on (BGa)(NAsP)-materials on silicon

R. Woscholski, C. Lammers, W. Stolz, M. Koch

Faculty of Physics and Material Sciences Center, Philipps-Universität Marburg

Introduction

The goal of my work performed in the framework of the GRK *functionalization of semiconductors* is to investigate the carrier dynamics of metastable nitrogenous and boracic III/V semiconductors on Silicon, fabricated in the framework of the GRK. The intention was to use the so called “pump-probe spectroscopy”, a powerful method with a high temporal and spectral resolution. To achieve this I did several preliminary measurements and setup modifications, which will be roughly outlined in this summary.

Work and Results

The band gap of the quantum well material lies at higher energies than the band gap-energy of the silicon substrate. As typical pump-probe measurements analyze the transmitted probe light, the spectral part that carries the absorption characteristics of the quantum wells will be absorbed when passing through the substrate.

As a first step two samples, grown on gallium phosphide, similar to those grown on silicon were studied to get some preliminary measurements for this material system that allow me to estimate the expectable absorption spectra and carrier dynamics. Given that the samples only consisted of three quantum wells, no absorption spectra could be obtained. Usually pump-probe measurements with the existing 1kHz system are done on samples with more than thirty quantum wells to improve the signal to noise ratio.

To perform future measurements on samples with more quantum wells grown on silicon one idea was to build a pump-probe setup that allows measurements in a reflective geometry. To test this new reflective pump-probe setup I used a well characterized germanium quantum well sample grown on silicon. The comparison with transmission pump-probe measurements revealed that both techniques show similar characteristic results, while the signal to noise ratio was much better for the transmission measurements. [Fig. 1] Due to the small differrences in the refractive indices between the different semiconductor materials most light was reflected at air-semiconductor interfaces, either at the front side of the sample (barrier-air interface) or at the back side (substrate-air interface) which means that in this kind of measurement most of the probe light still passes through the substrate.

Another requirement for good pump-probe measurements is a stable, spectral smooth probe pulse. I performed a characterization of the white light in the required wavelength range, using different sets of filters and an additional BBO-crystal. Acceptable results for the range of 450nm-750nm and for 850nm to 1000nm were achieved. [Fig. 2] The spectral region around 800nm still poses a challenge, due to the incident beam at 800nm, used for the self-phase modulation.

Conclusions

Most preparations and preliminary experiments are finished. To perform successful pump probe measurements samples with more quantum wells are needed. As the reflective pump-probe measurements bear no advantage over transmissive measurements, the best solution seems to be an entire removal of the substrate. Depending on the energetic position of the exzitonic resonances it might be necessary to assemble measurements with different probe light spectra.

Outlook

New samples with more quantum wells are fabricated by the WZMW. In order to use them in a pump-probe setup the substrate will be removed. I plan to investigate the carrier dynamics of this material system with the transmissive pump-probe setup. By varying the excitation wavelength and power, I will try to study the relaxation and scattering times and monitor scattering processes with a high temporal resolution.

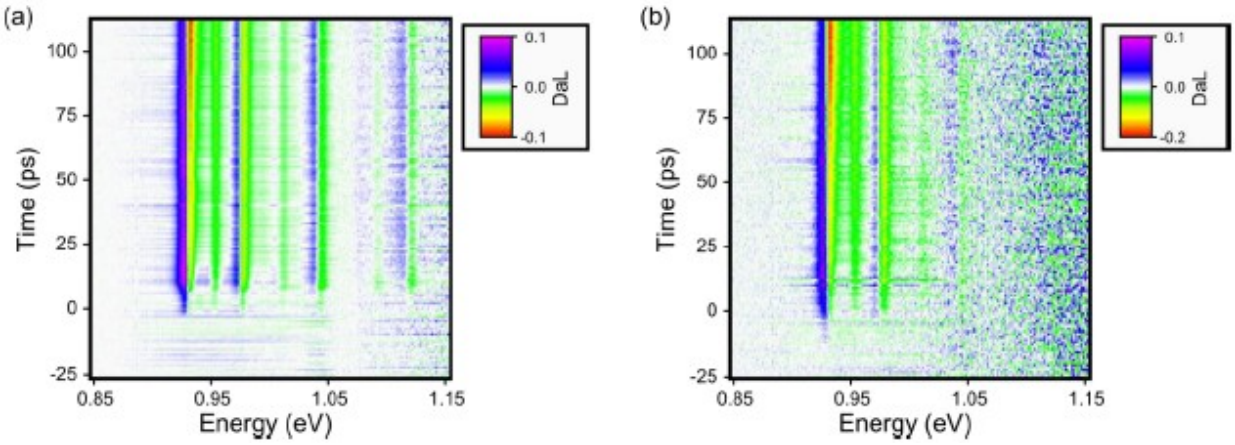

Figure 1: Pump-probe measurements on a germanium quantum well sample (a) in transmission, (b) in reflection

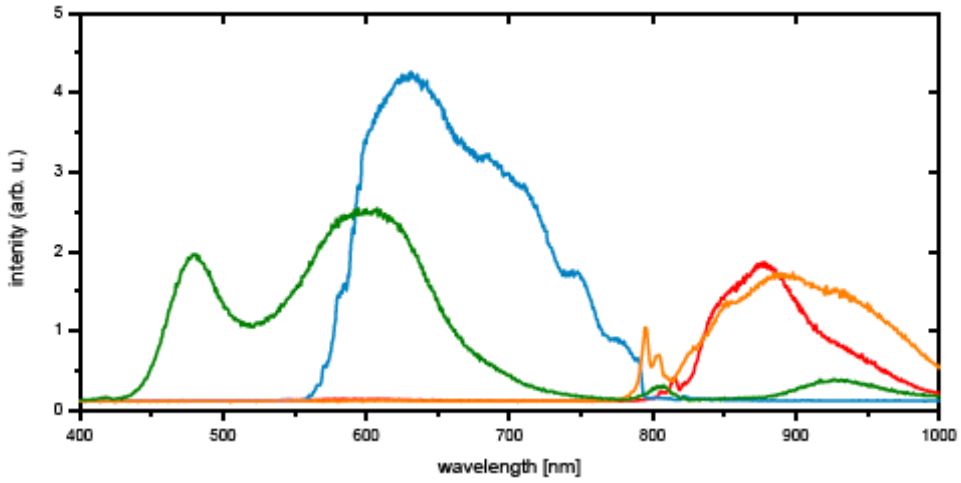

Figure 2: Different probe-pulse spectra that can be achieved by choosing different filter sets and/or the use of an additional BBO-crystal

THz Effects on the Polarisation in Quantum Wells

M. Drexler, R. Woscholski, S. Lippert, W. Stolz, M. Koch

Faculty of Physics and Material Sciences Center, Philipps-Universität Marburg

Introduction

The macroscopic dephasing time of an induced polarisation is an important quantity when analysing the material quality of an epitaxially grown material system. It is often regarded as the damping of the coherent response of a system and constitutes a crucial parameter when designing and modeling a Laser material.

Here we use the four-wave-mixing (FWM) technique [1] not only to measure these dephasing times, but we also employ an additional THz field to monitor the transient response of the polarisation to a fast external field with frequencies in the THz range. [1]

Results

The setup as shown in Fig. 1 has been realized with a 1 kHz femtosecond amplifier and tested on a multiple quantum well InGaAs/GaAsP structure grown by W. Stolz. We found a dephasing time of about 600 fs for the undisturbed case (Fig. 2 left). When the THz field is switched on, the overall intensity drops and the dephasing dynamics are disturbed depending on the time T_{THz}. At the same time, the spectral FWM signal is broadened (Fig. 2 right) which might be explained by ionization effects [2].

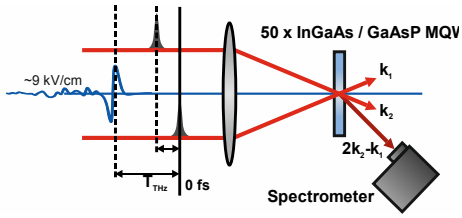

Fig. 1: *FWM setup with an additional THz pulse.*

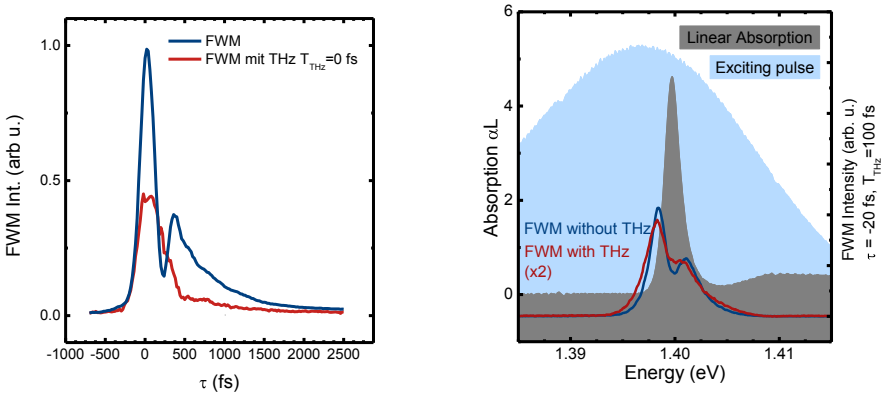

Fig. 2: *Exemplary results for time resolved (left) and spectrally resolved (right) FWM data (T = 7 K).*

Outlook

It is planned to extend this work from quantum wells to thin films of anorganic semiconductors, where propagation effects should dominate the systems answer. A set of thin films (GaAs and CdS) has been obtained and first measurements have been performed

[1] In [3] the possibility of on-chip modulators driven by a strong THz field is discussed.

on the GaAs film. At first the thickness of the film has been determined to about 1.1 µm, derived from the Fabry-Perot interference visible in a linear absorption experiment (Fig. 3).

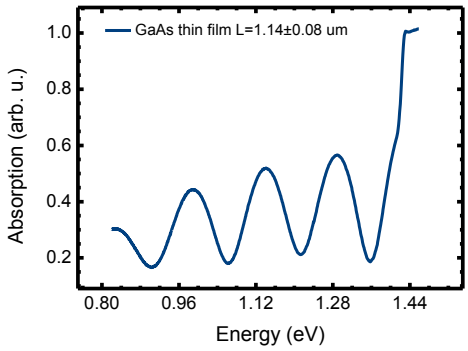

Fig. 3: *Thickness measurement of a thin GaAs film on Sapphire (T = 7 K).*

Further investigations should give a more detailed insight into the coupling effects between the (propagating) polarisation and an external THz field that might contribute to the topic of ultrafast light modulators [3].

[1] J. Feldmann, T. Meier, von Plessen G, M. Koch, E. Göbel, P. Thomas, G. Bacher, C. Hartmann, H. Schweizer, W. Schäfer, and H. Nickel, “Coherent dynamics of excitonic wave packets.,” *Physical review letters*, vol. 70, no. 20, pp. 3027–3030, May 1993.

[2] B. Ewers, N. Köster, R. Woscholski, M. Koch, S. Chatterjee, G. Khitrova, H. Gibbs, a. Klettke, M. Kira, and S. Koch, “Ionization of coherent excitons by strong terahertz fields,” *Physical Review B*, vol. 85, no. 7, pp. 1–5, Feb. 2012.

[3] R. Huber, “Terahertz collisions,” *Nature comm.*, vol. 483, pp. 545–546, 2012.

Theoretical Modeling of Semiconductor Materials and Semiconductor Systems

A. Bäumner and S. W. Koch

Department of Physics and Material Sciences Center,
Philipps-University of Marburg, Renthof 5, 35032 Marburg, Germany

1. Introduction

In this project, we aim at a detailed analysis of the optical properties of modern semiconductor materials and semiconductor systems on the basis of an established quantum-mechanical many-body theory.

Central components of this many-body theory are (i) the 8x8 k·p-theory for the computation of the electronic band-structure, (ii) the well-known semiconductor Bloch equations including the Coulomb-interaction coupling among excitonic excitations for the microscopic description of the linear optical response of a semiconductor material to a classical light-field and (iii) the semiconductor luminescence equations for the description of luminescence resulting from spontaneous recombination of electronic excitations taking into account the quantized light-matter interaction. Together, these equations allow a microscopic, quantitative computation of absorption- and gain spectra, refractive index changes, photoluminescence spectra and intrinsic charge carrier losses caused by radiative and non-radiative recombination processes. Thus, these equations may be consulted for material-characterization and device-optimization problems.

2. Project definition

Current issues and performance requirements demand problem-orientated modifications and a continuous further development of the approved theory.

In this context, for the project under consideration, the characterization and optimization of dilute nitride III-V semiconductor alloys is of special interest as, for instance, compound materials based on gallium nitride arsenide phosphide can be grown lattice-matched on silicon substrate and may thus bring off the industry-relevant silicon-based photonics-electronics integration in consequence.

The characterization and optimization of dilute nitride III-V semiconductor alloys, however, necessitates a modification of the computation and description of the electronic band-structure.The band-structure of these alloys, especially of III-V semiconductor compound materials with a nitride fraction of 0.5% to 8%, differs decisively from the band-structure of conventional semiconductor compounds. As due to their small size and relatively high electro-negativity the nitride anions distinguish themselves significantly from arsenic and phosphoric anions [1], respectively, nitride anions constitute local impurities within the crystal potential. The electronic level of these nitride induced iso-electronic impurities is resonant with the conduction band of the III-V semiconductor host-material [2] and thus strongly modifies the electronic band-structure at the conduction-band edge – an interrelationship which is described empirically within the framework of the band-anticrossing (BAC) model in terms of a coupling of the conduction-band states with the states of the localized nitride anions [3].

To go beyond the band-anticrossing model, the modification of description of the electronic band-structure in dilute nitride III-V semiconductor alloy is to be worked out carefully in iterative interaction with the co-operation partners in the field of theoretical chemistry and will need verification by the co-operation partners from experimental semiconductor physics.

Similarly to nitride, also bismuth induces iso-electronic impurities within a GaAs-host material as the electronegativity of bismuth atoms is far lower than the electronegativity of the substituted arsenic atoms [1]. However, the electronic level of the bismuth impurities is resonant with the valence bands of the semiconductor-host material, such that different from nitride admixtures bismuth admixtures do not lead to a modification of the electronic band-structure near the conduction-band edge but near the valence-band edges. Due to the possible emission wavelengths of Ga(AsBi) quantum-wells in a wide region stretching from near to medium infrared, this novel material system my find applications as gain material in diode-lasers with wavelengths of 1.3 µm and 1.55 µm, which are relevant for optical data transfer in telecommunication.

In first model computations of the optical properties of Ga(AsBi) quantum-wells, the BAC-model description of the electronic band-structure of dilute nitride III-V semiconductor alloys has been assigned to the description of the electronic band-structure of bismuth compounds by coupling the valence-band states of the host material to the states of the localized bismuth atoms using a valence-band anticrossing (VBAC) model [4-6].
In the present project, recent results of tight-binding computations [7] are considered and integrated step by step in the band-structure computation, to perform further model studies and conduct first experimental-theory comparisons to analyze the material system more closely.

References:

[1] RIEDEL, E.; JANIAK, C: *Anorganische Chemie (7. Auflage)*. De Gruyter Berlin, 2007

[2] HJALMARSON, H. P.; VOGL, P.; WOLFORD, D. J.; DOW, J. D.: Theory of Substitutional Deep Traps in Covalent Semiconductors. In: *Physical Review Letters 44* (1980). S. 810

[3] SHAN, W.; WALUKIEWICZ,W.; AGER, J. W.; HALLER, E. E.; GEISZ, J. F.; FRIEDMAN, D. J.; OLSON, J. M.; KURTZ, S. R.: Band Anticrossing in GaInNAs Alloys. In: *Physical Review Letters 82* (1999). S. 1221

[4] WU, J.; SHAN, W.; WALUKIEWICZ, W.: Band anticrossing in highly mismatched III-V semiconductor alloys. In: *Semiconductor Science and Technology 17* (2002), S. 860

[5] ALBERI, K.; WU, J.; WALUKIEWICZ, W.; YU, K. M.; DUBON, O. D.; WATKINS, S. P.; WANG, C. C.; LU, X.; CHO, Y.-J.; FURDYNA, J.: Valence-band anticrossing in mismatched III-V semiconductor alloys. In: *Physikal Review B 75* (2007, S. 045203)

[6] IMHOF, S.: *Mikroskopische Modellierung dichteabhängiger Photoreflexionsspektren in Halbleiterheterostrukturen*. Philipps-Universität Marburg, Diplomarbeit

[7] BRODERICK, C. A.; USMAN, M.; O'REILLY, E. P.: *Derivation of 12 and 14-band k.p Hamiltonians fordilute bismide and bismide-nitride semiconductors* (to be published (2013))

On the Phonon Interactions and Terahertz Excitations among Coulomb-correlated Charge Carriers of Semiconductors

C. N. Böttge,* M. Kira, and S. W. Koch

Department of Physics and Material Sciences Center,
Philipps-Universität Marburg, Renthof 5, 35032 Marburg, Germany

INTRODUCTION

In my PhD-thesis studies, a microscopic theory has been applied and extended to describe phonon-assisted processes [1–3] and terahertz excitations [4–6] in semiconductors. All investigations have been performed in the incoherent regime [7] where all coherent quantities vanish and the quantum nature of light [8] becomes important. Based on the Heisenberg equation-of-motion approach [9], the cluster-expansion scheme [10–13] has been adopted to truncate the infinite hierarchy of coupled equations. In this context, the arising expectation values are classified by recursively identifying correlated clusters [14]. By this means, the many-body hierarchy is systematically factorized into lower- and higher-order expectation values. As a result of the sequential buildup of correlated clusters, the procedure leads to a physical and intuitive interpretation of the clusters and the truncation scheme. In the presented microscopic theory, the generic structure of the cluster-expansion approach appeared to be very beneficial as it can be straightforwardly generalized to include new coupling effects without the necessity to reformulate the existing theory from scratch.

RESULTS

During my studies, I achieved considerable results and insights in the following three projects:

Enhancement of the phonon-sideband luminescence in semiconductor microcavities

In the first project, the semiconductor luminescence equations (SLEs) [7, 13, 15, 16] have been extended to include LO-phonon-assisted processes involving the first phonon sideband (PSB) arising at the low-energy side of the 1s-exciton resonance which is often referred to as the zero-phonon line (ZPL). For the description of photon-assisted polarizations in the incoherent regime where the calculation involves a completely quantized light field described by photon-creation and -annihilation operators, it is sufficient to truncate the hierarchy of coupled equations at the singlet–doublet level of the cluster-expansion scheme. However, extending this theory to describe also PSBs arising at the low-energy side of the ZPL leads to additional phonon-creation operators. In this context, the n^{th} PSB is described by $(n + 2)$-particle correlations such that the first PSB already invokes the triplet level of the cluster-expansion scheme. Consistently including stimulated-emission effects, a microscopic theory has been presented to describe phonon-assisted luminescence in a microcavity. Besides a full numerical evaluation of the phonon-assisted SLEs, a rigorous analytic model has also been developed. Here, the obstacles that arise from the stimulated parts in the SLEs could systematically be handled by introducing the *strong-cavity approximation*. This opened up the possibility to formulate a closed analytical formula to describe phonon-assisted luminescence in a cavity. In both, the numerical and the analytical computations, the standard scenario where the cavity resonance coincides with the 1s-exciton resonance, i.e., the ZPL, has been expanded by the option to freely tune the cavity resonance to any arbitrary frequency. This rendered investigations of different cavity configurations possible. On the one hand, normal-mode coupling for a cavity resonant with the ZPL was observed but, on the

other hand, a new effect could also be identified where the PSB is highly enhanced if the cavity resonance is shifted to coincide with the first phonon-sideband resonance. Intensity studies in dependence of the quality of the cavity indicate an initial increase of the luminescence intensity due to the Purcell effect [17], followed by a subsequent decrease as the system transitions into the nonperturbative regime, if the cavity is resonant with the ZPL. For a cavity resonant with the first PSB, the integrated luminescence saturates which reveals qualitative changes in the cavity effects and the impact of a detuned microcavity on the system properties. These results have been published in Refs. [18, 19].

An additional study on the participation of electron–hole plasma and exciton sources has been published in Ref. 20.

Phonon-assisted luminescence of polar semiconductors

As already investigated in the first project, the interaction between electrons and longitudinal-optical (LO) phonons gives rise to pronounced PSBs in the luminescence spectrum. This interaction may be modeled by either the short-ranged optical deformation-potential scattering or the long-ranged Fröhlich interaction which exists in polar media. In order to identify the origin of exciton–phonon interaction in polar semiconductors, time-resolved photoluminescence spectroscopy has been used to investigate the PSBs of three polar, wide-gap materials, namely ZnO, ZnS, and CdS, as a function of temperature and excitation density. The experimental results have been confirmed by a theoretical many-body approach where the relative contributions of Fröhlich interaction and optical deformation-potential scattering were identified. Here, a steady-state luminescence formula has been developed to investigate exciton-population-dominated first (PSB_1) and second (PSB_2) phonon-sideband luminescence. For low densities where correlated emission sources prevail, the exciton picture constitutes a suitable formulation for the description of PSBs, as the hierarchy problem that arises from the Coulomb interaction is eliminated in this representation. The experiment–theory comparison has demonstrated that many-body interactions significantly influence the phonon-interaction mechanisms. While Fröhlich interaction governs the scattering in CdS, deformation-potential scattering prevails in ZnO. In ZnS, both processes contribute equally. As an important fact, the theoretical studies have shown that scattering between *single electrons* and an optical phonon is dominated by the Fröhlich interaction in all three investigated materials. However, the strong Coulomb coupling between electrons and holes leads to strong suppression of the Fröhlich interaction, particularly in ZnO, such that optical deformation potential is here the overall dominant mechanism that is responsible for the sideband emission. These results have been published in Ref. 21.

Magnetic-field control of terahertz and Coulomb interactions among excitons

The studies on the exciton–phonon interaction have demonstrated that Coulombically bound electron–hole pairs, i.e., excitons, have pronounced effects on the optical properties of semiconductors. After creation of polarizations, carriers, and correlations in the semiconductor via an optical interband excitation using visible or near-infrared (NIR) light, some fraction of the excited carriers may bind into excitons. As the energy spacing between intra-exciton transitions is in the terahertz (THz) range, THz spectroscopy is ideally suited to probe correlated semiconductor many-body states and to induce controlled transitions between the different states [22]. In contrast to interband processes, intraband transitions do not alter the number of total excited carriers. Recently, the THz-induced, dipole-forbidden 1*s*-to-2*s* transition has been reported, which could be traced back to the diffusive Coulomb scattering among 1*s*, 2*p*, and 2*s* states [23]. Based on these studies, the influence of an external magnetic field on

THz transitions and Coulomb scattering has been investigated in the third project. A magnetic field significantly alters the properties of excitons such as the eigenenergies and wavefunctions. However, the internal energy spacing between different exciton states remains in the THz regime such that THz spectroscopy is still in demand when a magnetic field is applied. As the Coulomb scattering induces intra-exciton transitions, the variations of the exciton properties induced by a magnetic field enable major control of the scattering among exciton states. Using time-resolved photoluminescence measurements of GaAs/AlGaAs multiple quantum wells, the dynamics of excitons have been probed via excitation using narrow-band THz pulses resonant with the dipole-allowed 1*s*-to-2*p* intra-exciton transition. The experimental findings have been corroborated by a theoretical model by fully including linear and nonlinear magnetic-field contributions to the total-system Hamiltonian. The magnetic field varies the exciton eigenvalues and eigenfunctions, and with this the THz-induced, Coulomb-mediated intra-exciton transitions and exciton-population dynamics. Besides significant changes in the co-operative interaction of Coulomb scattering and THz field, both experiment and theory could reveal additional THz-induced transitions to higher exciton states which would not be observable without a magnetic field. As a very intriguing result, it could be shown that the system becomes few-level-like when a magnetic field is applied. The manuscript for this project is currently in preparation and will be submitted soon.

CONCLUSIONS

In summary, I have worked on three projects of two different fields of research. While the first two projects concentrated on studies of phonon sidebands arising in the semiconductor luminescence, the third project was dedicated to the investigation of the impact of a magnetic field on the exciton-correlation dynamics, the diffusive Coulomb scattering, and the THz-transition probabilities in correlated semiconductor many-body systems. All project produced interesting results and provided major insights into the processes of interacting many-body systems. In total, six research papers with my participation as the first or a co-author, i.e., Refs. [5, 6, 18–21], have been published in peer-reviewed journals. One manuscript is currently in preparation and will be submitted in the near future.

OUTLOOK

Just recently, I started a project in collaboration with Prof. Yun-Shik Lee from the Oregon State University, Corvallis, OR (USA), where cavity-beating effects of exciton–polariton modes in Λ-type three-level systems are investigated. Taking advantage of the fact that THz radiation only couples to the polarization but not directly to the electric field, the beating of the energy oscillating between optical field and 1*s* polarization could be determined by varying the THz arrival time with respect to the optical field. This results in spectro-temporal interference patterns in the optical reflectivity. The results of this project are currently summarized and the manuscript is intended to be published soon.

* Christoph.Boettge@physik.uni-marburg.de

[1] T. Feldtmann, *Influence of phonons on semiconductor quantum emission*, Ph.D. thesis, Philipps-Universität Marburg, Department of Physics and Material Sciences Center, Marburg (Germany) (2009).
[2] T. Feldtmann, M. Kira, and S. Koch, J. Lumin. **130**, 107 (2010).
[3] T. Feldtmann, M. Kira, and S. W. Koch, Phys. Status Solidi B **246**, 332 (2009).

[4] J. T. Steiner, *Microscopic Theory of Linear and Nonlinear Terahertz Spectroscopy of Semiconductors*, Ph.D. thesis, Philipps-Universität Marburg, Department of Physics and Material Sciences Center, Marburg (Germany) (2008).
[5] C. N. Böttge *et al*., Phys. Status Solidi C, *accepted* (2013), DOI: 10.1002/pssc.201200702.
[6] C. N. Böttge *et al*., Phys. Status Solidi B, *accepted* (2013), DOI: 10.1002/pssb.201200704.
[7] M. Kira and S. W. Koch, Prog. Quantum Electron. **30**, 155 (2006).
[8] S. W. Koch, M. Kira, G. Khitrova, and H. M. Gibbs, Nature Mater. **5**, 523 (2006).
[9] H. Haug and S. W. Koch, *Quantum Theory of the Optical and Electronic Properties of Semiconductors*, 5th ed. (World Scientific, Singapore, 2009) – ISBN 981-283-883-X.
[10] J. Fricke, Ann. Phys. (NY) **252**, 479 (1996).
[11] M. Kira and S. W. Koch, Eur. Phys. J. D **36**, 143 (2005).
[12] M. Kira and S. W. Koch, Phys. Rev. A **78**, 022102 (2008).
[13] M. Kira and S.W. Koch, *Semiconductor Quantum Optics*, 1st ed. (Cambridge Univ. Press, Cambridge (England, UK), 2011) – ISBN 978-0-521-87509-7.
[14] M. Mootz, M. Kira, and S. W. Koch, J. Opt. Soc. Am. B **29**, A17 (2012).
[15] M. Kira *et al*., Phys. Rev. Lett. **79**, 5170 (1997).
[16] M. Kira *et al*., Prog. Quantum Electron. *23*, 189 (1999).
[17] E. M. Purcell, Phys. Rev. **69**, 681 (1946).
[18] A. Chernikov, C. N. Böttge, T. Feldtmann, S. Chatterjee, M. Koch, M. Kira, and S. W. Koch, Phys. Status Solidi C **8**, 1129 (2011).
[19] C. N. Böttge, M. Kira, and S. W. Koch, Phys. Rev. B **85**, 094301 (2012).
[20] C. N. Böttge, T. Feldtmann, M. Kira, and S.W. Koch, Phys. Status Solidi C **8**, 1220 (2011).
[21] A. Chernikov, V. Bornwasser, M. Koch, S. Chatterjee, C. N. Böttge, T. Feldtmann, M. Kira, S. W. Koch, T. Wassner, S. Lautenschläger, B. K. Meyer, and M. Eickhoff, Phys. Rev. B **85**, 035201 (2012).
[22] M. Kira, W. Hoyer, and S. W. Koch, Solid State Commun. **129**, 733 (2004).
[23] W. D. Rice, J. Kono, S. Zybell, S. Winnerl, J. Bhattacharyya, H. Schneider, M. Helm, B. Ewers, A. Chernikov, M. Koch, S. Chatterjee, G. Khitrova, H. M. Gibbs, L. Schneebeli, B. Breddermann, M. Kira, and S. W. Koch, Phys. Rev. Lett. **110**, 137404 (2013).

Microscopic Modeling of Optically Excited Semiconductor Heterostructures

Benjamin Breddermann[1]

[1] *Faculty of Physics and Material Sciences Center, Philipps-Universität Marburg*

Exposé

So far, my PhD project with the working title *Mikroskopische Modellierung optisch angeregter Halbleiterheterostrukturen* (engl.: *Microscopic modeling of optically excited semiconductor heterostructures*) was closely connected to the topic of my diploma thesis entitled *Many-body effects in Terahertz-spectroscopy of semiconductors*, which I already produced in the semicodcuctor theory group of the physics department in Marburg.

Within the framework of those projects, I worked on the investigation of scattering mechanisms in semiconductor quantum wells, in order to develop a microscopic understanding of the appearing broadening and dephasing effects of the excitonic resonances in the resulting absorption spectra.

A particlular focus in the investigation of the involved many-particle effects is put on the analysis of the terahertz response of the optically excited system. Spectroscopically, the Coulomb scattering effects showing up under terahertz excitation can be detected via the evaluation of the resulting time-resolved photoluminescence. The findings concerning these studies have already been experimentally verified and documented in publications [3, 4].

The additonal influence of a magnetic field with respect to intraexcitonic transitions was already treated in publication [2] and is - with the aim of more specific focus on the scattering effects - still object of current research.

Within the continuation of my PhD studies being now a fellow (german: *Kollegiat*) of the *Graduiertenkolleg* entitled *Funktionalisierung von Halbleitern* I want to shift my main research focus more to the application-related simulation of the optoelectronic properties of specific – particularly dilute – semiconductor material systems. Thereby, e.g., the investigation of the gain properties is of particular interest - especially with respect to laser applications [1].

Besides the understanding of dilute nitride semiconductor materials, which are already quite well-examined both theoretically and experimentally, the better understanding of the effects which are induced by the incorporation of a dilute bismut concentration, are still an important topic of current research. On the basis of recently measured experimental data this new project is the starting point for a couple of theoretical simulations based on well-established approaches and methods for the microscopic modeling of the optical response of the respecttive semiconductor material structures.

For such kind of projects, which need a close cooperation between experimental and theoretical physics, the interdisciplinary networking within the framework of the *Graduiertenkolleg* provides an optimal basis.

Work schedule:

- June 2013: initial skill adaption for new project (simulation of dilute bismide semiconductors)
- June 2013 – December 2013: simulation of specific dilute bismide semiconductor material systems, theory-experiment-comparison based on recent measurements
- January 2014 – May 2014: Working on PhD thesis taking into account both the old (scattering mechanisms) and the new (semiconductor material systems) complex of themes.

References

[1] Christina Bückers. *Mikroskopische Analyse optoelektronischer Eigenschaften von Halbleiterverstärkungsmedien für Laseranwendungen*. Dissertation, Universtiätsbibliothek Marburg, 2010.

[2] C. N. Böttge, B. Breddermann, L. Schneebeli, M. Kira, S. W. Koch, J. Bhatacharyya, H. Schneider, and M. Helm. *Terahertz-induced effects on excitons in magnetic field*. Phys. Status Solidi C, accepted, 2013.

[3] C. N. Böttge, S. W. Koch, L. Schneebeli, B. Breddermann, A. C. Klettke, M. Kira, B. Ewers, N. S. Köster, and S. Chatterjee. *Terahertz-induced exciton signatures in semiconductors*. Phys. Status Solidi B, accepted, 2013.

[4] W. D. Rice, J. Kono, S. Zybell, S. Winnerl, J. Bhattacharyya, H. Schneider, M. Helm, B. Ewers, A. Chernikov, M. Koch, S. Chatterjee, G. Khitrova, H. M. Gibbs, L. Schneebeli, B. Breddermann, M. Kira, and S. W. Koch. *Observation of forbidden exciton transitions mediated by coulomb interactions in photoexcited semiconductor quantum wells*. Phys. Rev. Lett., 110:137404, 2013.

CdSe/ZnS core shell QDs modified electrode as a Photochemical Sensor for the Sarcosine

Abuelmagd M. Abdelmonem[a], Marc Riedel[b], Gero Göbel[b], Wolfgang J. Parak[a], Fred Lisdat[*,b]

[a] Biophotonik, Philipps-Universität Marburg, Marburg, Germany
[b] Biosystems Technology, Wildau Technical University of Applied Sciences, 15745 Wildau Germany

Introduction

Photoelectrochemical sensors and biosensors based on the Qdots nanocrystals are among the most promising alternatives for the detection of chemicals and biochemical molecules in the industrial, environmental and biological applications compared to other sensor types. These QDs based photochemical sensors have been extensively investigated during the last few years. In these sensors, the QDs are immobilized by a linking molecule (linker) on the electrode surface, so that upon the illumination, a photocurrent is generated. The generated photocurrent depends on the type and concentration of the respective analyte in the immediate environment of the electrode.

In present study, a sarcosine photoelectrochemical sensor based on the CdSe/ZnS core shell QDs is reported. To achieve this purpose, 1,4-benzenedithiol capped CdSe/ZnS core shell QDs were prepared then electrodes were modified by are prepared and the dependence of photocurrent on the oxygen is evaluated under illumination[(1-8)].

Results

The photocurrent can be suppressed in the presence of the sarcosine oxidase (SOD) because of biocatalytic oxygen reduction.

To construct the photoelectrochemical sensor, SOD is immobilized on the surface of QDs modified electrode using the multilayer assembly technique using a polyelectrolyte poly(allylamine hydrochloride) (PAH). Multi-layer systems of up to six bilayers have been built up through the electrostatic interaction. The assembly can be verified by surface plasmon resonance measurements. The influence of varying the number of bilayers and the amount of enzyme on the sensitivity of the photoelectrochemical sensor can be shown. Using [SOD/PAH]6-bilayers system resulted in a signal change of 0.041 % μM^{-1} in the linear range of 100 µM to 1 mM of sarcosine.

Conclusion

Fabrication and applications of CdSE/ZnS core shell QDs and light-directed read-out based photoelectrochemical sensor have been described for sarcosine as an example for biochemical detection.

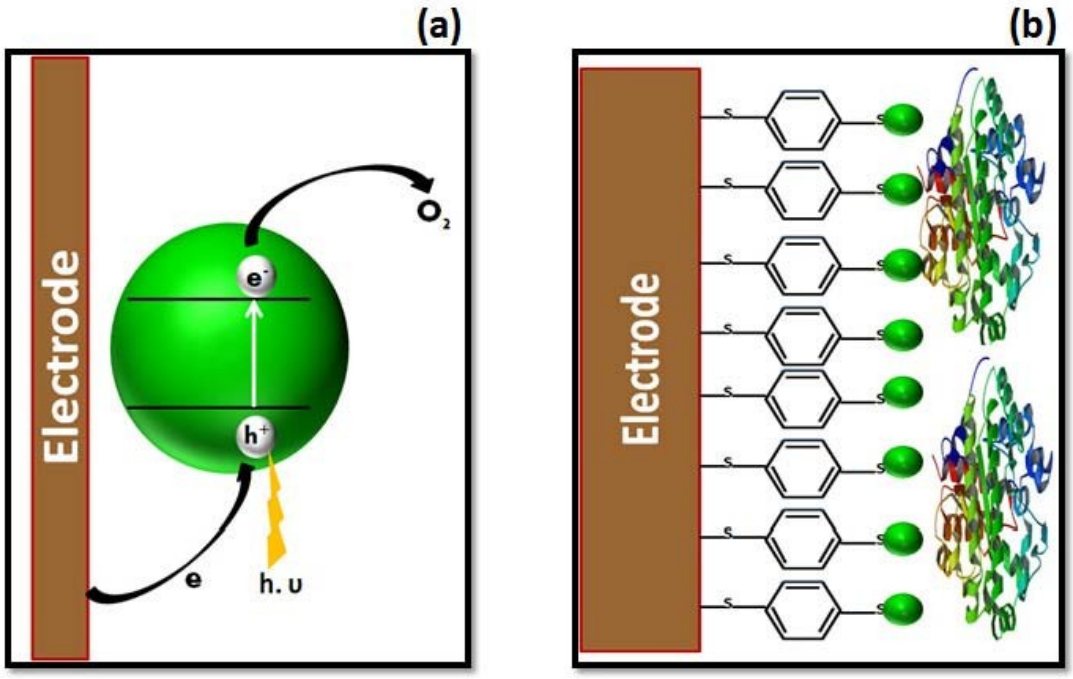

Illustration of the electron transfer steps at the QD-electrode (a) and the layer by layer assembly of the [SOD/PAH]-bilayer on a 1,4-Benzenedithiol modified electrode (b).

References

1. Yue, Z., Khalid, W., Zanella, M., Abbasi, A. Z., Pfreundt, A., Rivera Gil, P., Schubert, K., Lisdat, F., Parak, W. J., 2010. Anal. Bioanal. Chem. 396, 1095-1103.
2. Moritz, W., Gerhardt, I., Roden, D., Xu, M., Krause, S., 2000. Fresensius J. Anal. Chem. 367, 329-333.
3. Stoll, C., Gehring, C., Schubert, K., Zanella, M., Parak, W. J., Lisdat, F., 2008. Biosens. Bioelectron. 24, 260-265.
4. Stoll, C., Kudera, S., Parak, W. J., Lisdat, F., 2006. SMALL 2, 741-743.
5. Tanne, J., Schäfer, D., Khalid, W., Parak, W. J., Lisdat, F., 2011. Anal. Chem. 83, 7778-7785.
6. Yoshinobu, T., Iwasaki, H., Ui, Y., Furuichi, K., Ermolenko, Y., Mourzina, Y., Wagner, T., Näther, N., Schöning, M. J., 2005. Methods 37, 94-102.
7. Koberling, F., Mews, A., Basché, T., 2001. Adv. Mater. 13, 672-676.
8. Katz, E., Zayats, M., Willner, I., Lisdat, F., 2006. Chem. Commun. 13, 1395-1397.

Work summary in the framework of the GRK Project 1782

Karsten Kantner

Faculty of Physics, Biophotonics Workgroup, Philipps-Universität Marburg

Introduction:
In the framework of the GRK Project 1782 we were introduced to both a scientific research project as well as access to a verity of lectures and seminars to improve the inter-scientific exchange between groups. The responsibility of the Biophotonics workgroup is to provide semiconductor nanoparticles with exact surface compositions and ligands as well as distinctive characteristics like the net charge for example. Therefore the surface characteristics as well as different compositions have to be tested, measured in a model system and proven before the use in the actual project.

Results:
The results that far were all coming from a Gold-nanoparticle (AuNP) system to prove the concept of surface and shape control. For that reason the AuNP system was created using very distinct surface charges as well as an overall very controlled size and shape distribution. The AuNPs were therefore a good prove of concept approach which can be transferred to the more complex semiconductor nanoparticles which will be used in the GRK project. Other ligands as well as different surface characteristics were also modified and altered to prepare for the final semiconductor nanoparticles.
As another, slightly tighter approach semiconductor nanoparticles were used on cells grown on top of a silicon chip. Thereby testing the usability and characteristics of said nanoparticles in different areas.

Conclusions:
All in all it can be said that the control system with the AuNPs proved to be a good approach, but only as prove of concept concerning the diversity of the particles themselves as well as their ability to be altered and shaped to perfect usability. There are a lot of possible transferable aspects from the AuNPs to the semiconductor nanoparticles. Therefore the use of AuNPs led to the conclusion that the nanoparticles for the GRK project can also be created and specified to nearly every desired purpose.

Outlook:
In the near future, the information gained by the control system will be used to improve or even create the desired semiconductor nanoparticles with the needed surfaces and ligands as well as material compositions.

References:

Hühn et.al.; Polymer-Coated Nanoparticles Interacting with Proteins and Cells: Focusing on the Sign of the Net Charge, ACS Nano, 04/2013

Synthesis and characterization of Mn-CdS/ZnS Nanoparticles:

N. Sabir, P. del Pino, W. J. Parak

Faculty of Physics, Philipps Universität Marburg, Renthof 7, 35032 Marburg

In last decade, Mn doped CdS/ZnS nanocrystals (NCs) have attracted much attention due to its optical and opto magnetic properties. Magnetic doped based NCs are suitable for different technological applications, in numerous fields such as biomedical diagnosis, solar cells, spin-tronics, light emitting diodes (LED) [1-7]. Mn dopants cause new photoluminescence features in nanocrystals, enabling particles with duel emission [1-8]. Doping with just few Mn^{2+} ions inside the ZnSe, ZnS and CdSe nanocrystals have been demonstrated to produce a large Zeeman effect [1-9]. Synthesis and characterization of Mn-doped CdS/ZnS core/shell nanocrystals, using a method described previously by Yang et al., are discussed.

Refrences.

1. M. Shim, C. Wang, D. J. Norris, P. Guyot-Sionnest, MRS Bull.2001, 1005.
2. J. D. Bryan, D. R. Gamelin, Prog. Inorg. Chem. 2005, 54, 47.
3. D. J. Norris, A. L. Efros, S. C. Erwin, Science 2008, 319, 1776.
4. D. Magana, S. C. Perera, A. G. Harter, N. S. Dalal, G. F. Strouse, J. Am. Chem. Soc. 2006, 128, 2931.
5. N. Pradhan, D. Goorskey, J. Thessing, X. Peng, J. Am. Chem. Soc. 2005, 127, 17586.
6. D. J. Norris, N. Yao, F. T. Charnock, T. A. Kennedy, Nano Lett.2001, 1, 3.
7. A. Nag, S. Chakraborty, D. D. Sarma, J. Am. Chem. Soc. 2008,130, 10605.
8. S. E. Irvine, T. Staudt, E. Rittweger, J. Engelhardt, S. W. Hell, Angew. Chem. 2008, 120, 2725; Angew. Chem. Int. Ed. 2008, 47, 2685.
9. Y. A. Yang, O. Chen, A. Angerhofer, Y. C. Cao, Chem. Eur. J.2009, 15, 1386.
10. Yang et. al., *J. Am. Chem. Soc*; 2008, *130* (46), Pages: 15649–15661

Deposition and physical characterization of graphene-like films on a Si-(001) surface

Katharina Werner

Material Sciences Center and Faculty of Physics, Philipps-Universität Marburg

My research in the framework of the GRK „Functionalization of Semiconductors" aims on the direct deposition of graphene on Si-(001) by chemical vapor phase deposition (CVD). Graphene exhibits a variety of extraordinary physical properties making it an interesting material for fundamental research and applications. Nowadays there are a few ways to produce graphene, namely the so-called scotch tape method[1] or the graphitization of silicon carbide, but those exhibit drawbacks like low controllability or the requirement for high growth temperatures, respectively. First attempts of direct deposition of graphene on a clean Si-(001) surface by CVD have not been successful[2], but CVD growth has been realized on metal substrates[3]. Our approach is to pre-treat the silicon surface by first depositing metallic gallium droplets, which we expect to have a catalytic effect on the decomposition of the carbon precursors and the graphene growth.
All samples were grown in a commercial metal organic vapor phase epitaxy reactor system. Different carbon precursors, namely 3,3-dimethylbut-1-ene, 3,3-dimethylbut-1-yne or benzene, were used. For carbon deposition growth temperatures were varied between 400°C and 800°C with growth times between 1 min and 10 min. Triethylgallium (TEGa) was used as a precursor for gallium deposition with growth times between 1 s and 15 s and growth temperatures between 375°C and 450°C. From earlier results on GaP it is known, that at 450°C growth temperature this corresponds to 0.1 to 1.5 monolayers of gallium for the chosen partial pressure and growth times. Samples were characterized by atomic force microscopy, transmission electron microscopy and energy dispersive X-ray spectroscopy, scanning electron microscopy and Raman spectroscopy.

First, the surface after deposition of TEGa at a growth temperature of 450°C was analyzed. AFM measurements, as shown in figure 1, revealed spots on the silicon surface with a height between 1 nm and 10 nm for the growth times between 1 s and 15 s.

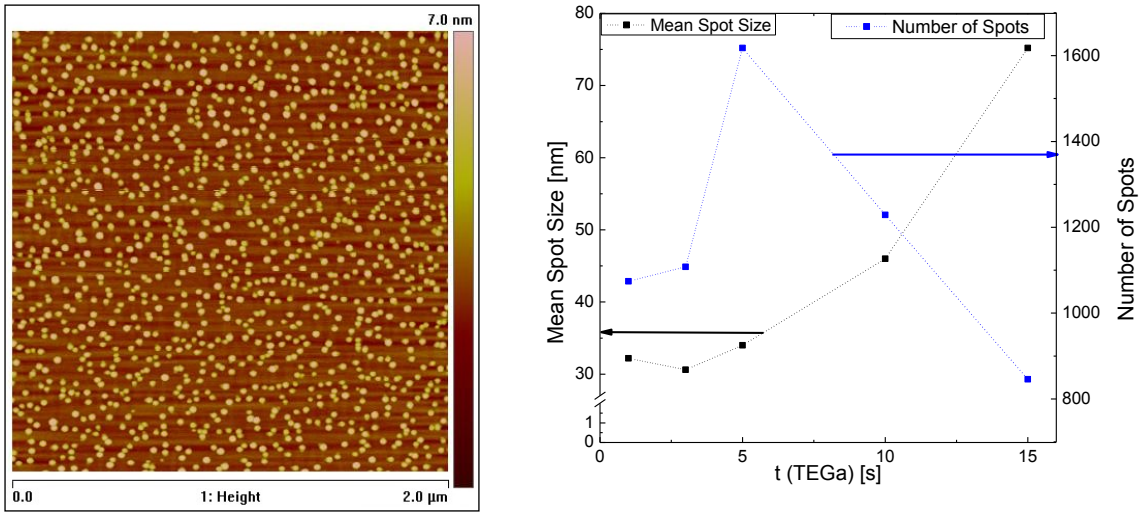

Fig.1: Atomic force microscope (AFM) image of the Si surface after 15 s of gallium deposition and the dependence of spot size and number on growth time

It was observed, that with increasing growth time the amount of spots increased in the beginning, while the spot size stayed rather constant. For longer growth times the spot size drastically increased while the number of spots decreased. This can be explained by small spots merging into combined large spots.

High-angle annular dark-field scanning transmission electron microscope (HAADF STEM) images of the samples after gallium deposition reveal that the gallium is not deposited on the silicon surface but etches into the silicon, building triangular structures with boundaries on the silicon (111) planes. In addition the surface is covered with an amorphous layer. Images of an identically grown sample after annealing at 800°C for 1 min show that no detectable amount of gallium is left at the surface, with the gallium either desorbing from the surface or defusing further into the silicon at those temperatures. This implies that carbon deposition has to be carried out at rather low temperatures when gallium is used as a catalyst.

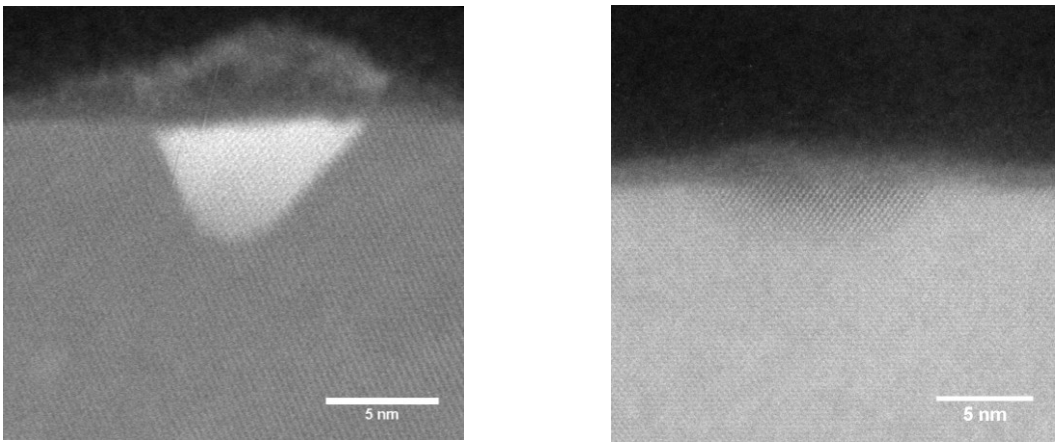

Fig.2: HAADF STEM images of the Si surface after gallium deposition at 450°C and after annealing an identically grown sample at 800°C for 1 min

Based on those results, the gallium deposition was performed at lower growth temperatures and for shorter growth times for later samples. We expect that with varying the growth parameters in this way the gallium will etch into the silicon less and more gallium will stay on the surface being able to act as a catalyst. First results support this thesis. To prevent the influence of high temperatures on the gallium shown in figure 2, carbon deposition was only carried out at growth temperatures of 400°C or 450°C for later samples. AFM images of those samples clearly show that carbon can be deposited on the gallium pretreated surfaces for the chosen growth parameters. This is a first step towards the growth of controllable graphene films, although Raman spectroscopic measurements reveal that no ordered carbon structures were deposited yet.

As the presence of a metallic catalyst is thought to be required for a controllable graphene growth on silicon, it is necessary for our approach to firstly understand the microscopic processes during the gallium deposition on Silicon (001) and optimize the growth parameters for metallic gallium droplets. As a next step the growth parameters for a controlled graphene film should be optimized and the films characterized in dependence of those parameters.

[1]K.S. Novoselov, et al. “Electric field effect in atomically thin carbon films.” Science 306, 666 (2004).

[2]B.J. Müller. “Herstellung und Charakterisierung von epitaktischem Graphen auf präparierten Si(001)-Oberflächen.“ Diploma thesis, Philipps Universität Marburg (2011)

[3]P.W. Sutter. “Epitaxial graphene on ruthenium”. Nature Materials 7, 406 (2008)

Coordination Chemistry and Redox Activity of Anthraquinone-Based Photo Sensitizer Ligands for DSSCs

Christian Prinzisky, Jörg Sundermeyer

AG Sundermeyer, Fachbereich Chemie, Philipps-Universität Marburg

A cost-efficient alternative to III-V-semiconductor and silicon-based solar cells is - due to lower material and production costs[1] - the dye-sensitized solar cell (DSSC) - also called GRÄTZEL-cell - which was developed in the early 1990^s by M. GRÄTZEL.[2] The core component of DSSCs is a photo sensitizer which absorbs photons and thereby undergoes a transition to an excited state. The excited electron can then be transferred to the conduction band of the covalently bound wide band gap semiconductor so that the electron is available as electric energy. Currently popular dye-sensitized solar cells are based on ruthenium(II)-polypyridine complexes and achieve efficiencies up to 11%.[3-5]

Alizarin, an anthra-9,10-quinone derivative and the dye of the madder root, which was already used as coloring agent in the Ancient Egypt, is known in form of its Ca-Al-complex as Turkish-red and is characterized by its brilliance and color fastness.[6] Anthraquinones usually have high molar extinction coefficients and strong absorption bands in the visible light range.[7] These properties make anthraquinone derivatives interesting for the use in dye-sensitized solar cells.[5]

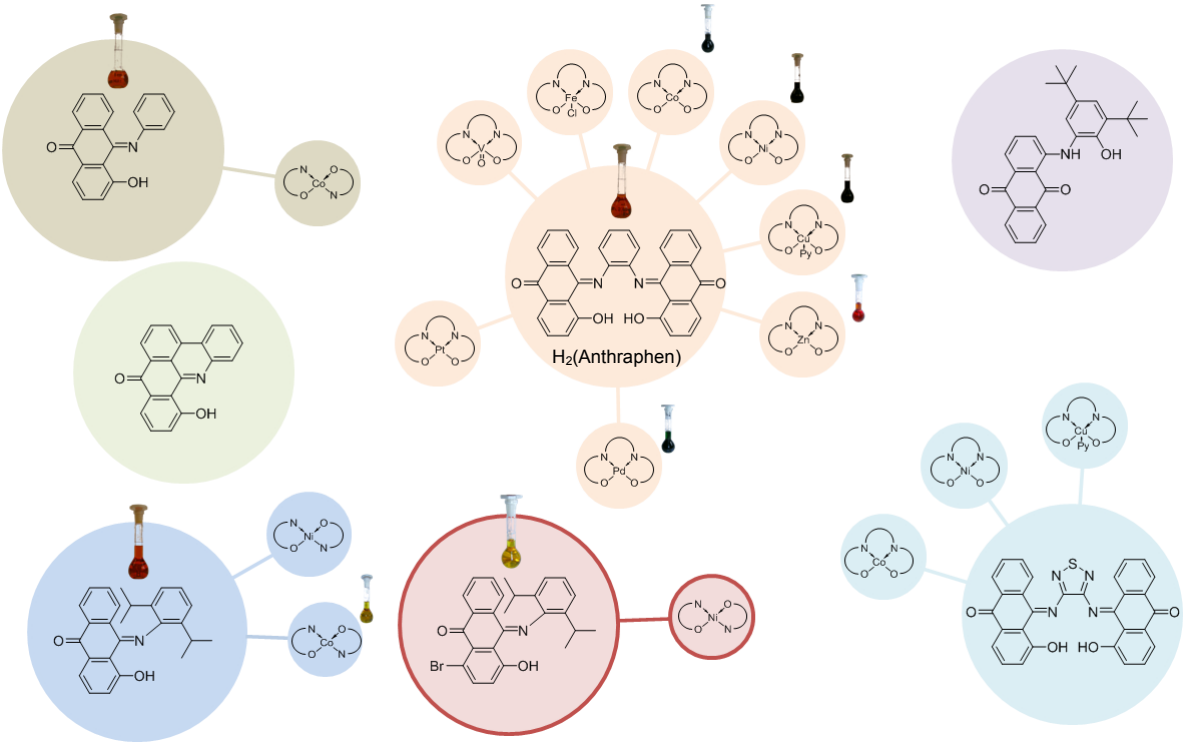

Figure 1: Overview of selected anthraquinone-based ligands and their complexes.

By condensation reactions of anthraquinonoid precursors like 1-hydroxy-9,9-dimethoxy-10-anthrone with primary amines such as *ortho*-phenylendiamine, 3,4-diamino-1,2,5-thiadiazole, aniline or 2,6-di*iso*propylaniline it is possible to synthesize various N,O-, N,O_2- and N_2,O_2-ligands. These ligands can be coordinated by reaction with various metal cations. Depending on the cation the correlated acetates, acetylacetonates or amides can be used as metalating

agents. An overview of selected anthraquinone-based ligands and their complexes is shown in figure 1. The colors of the discs show qualitatively the optical characteristics of the respective compound.

The electrochemical properties of the ligands and complexes are examined by cyclic voltammetry. It provides information about the reversibility of the occurring redox processes and the electrochemical stability of the analyzed compound. Also a qualitatively interpretation of the observed processes is possible. Figure 2 exemplify the cyclic voltammogram of [Co^{II}(Anthraphen)] and the comparison of the UV/VIS spectra of H_2(Anthraphen) and [Co^{II}(Anthraphen)] in dichloromethane. The molar extinction coefficients of the complex reach values up to 70,000 $L \cdot mol^{-1} \cdot cm^{-1}$.

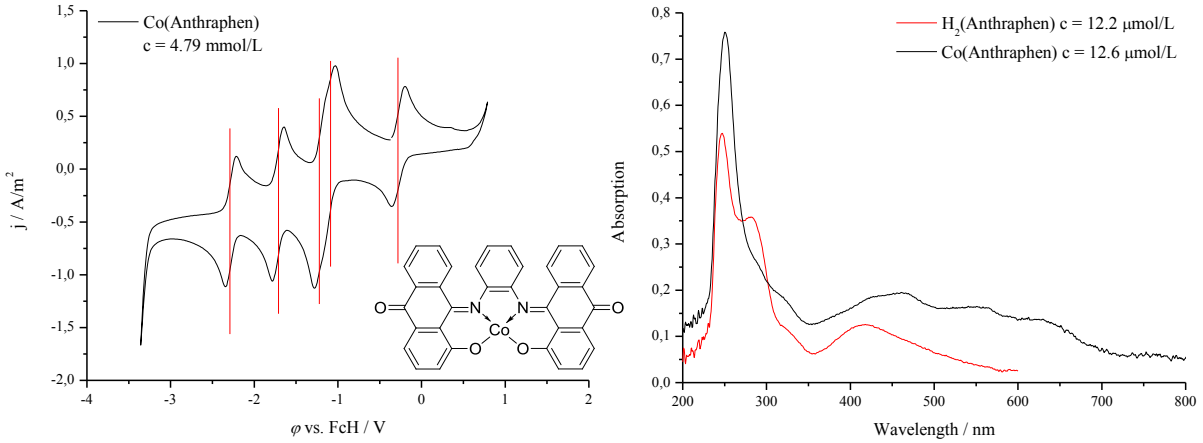

Figure 2: left: Cyclic voltammogram of [Co^{II}(Anthraphen)] in DMSO (conducting salt: [TBA]PF_6, working electrode: glassy carbon, counter electrode: Pt, reference electrode: Pt, reference: FcH); right: Comparison of the UV/VIS spectra of H_2(Anthraphen) and [Co^{II}(Anthraphen)] in dichloromethane.

The high stability against multiple reduction is remarkable. Thus, four reversible redox processes are observed in the anodic region. The high stability against reduction and oxidation, a tunable redox potential, and high extinction coefficients in the visible light range are prerequisites for the application in dye-sensitized solar cells. In further work N,O-ligands should be synthesized and complexed starting from 1-chloroanthra-9,10-quinone or 1-aminoanthra-9,10-quinone by reactions with amines or carbonyl derivatives. Furthermore the attachment of a carboxyl group as an anchor group for the immobilization on oxidic semiconductors such as ZnO and TiO_2 might support the application in DSSCs.

[1] M. Grätzel, *Nature* **2001**, *414*, 338-344.
[2] B. O'Reagan, M. Grätzel, *Nature* **1991**, *353*, 737-740.
[3] A. Hagfeldt, M. Grätzel, *Inorg. Chem.* **2005**, *44*, 6841-6851.
[4] M. Grätzel, *Acc. Chem. Res.* **2009**, *42*, 1788-1798.
[5] C. Prinzisky, Masterarbeit, *Philipps-Universität Marburg*, **2011**.
[6] H. M. Koch, P. Pfeifer, *NiU-Chemie* **1999**, *10*, 25-26.
[7] C. Li, X. Yang, R. Chen, J. Pan, H. Tian, H. Zhu, X. Wang, A. Hagfeldt, L. Sun, *Sol. Energy Mater. Sol. Cells* **2007**, *91*, 1863-1871.

Towards Novel Redox Mediators for Dye-sensitised Solar Cells

Lars Hendrik Finger

AK Sundermeyer, FB Chemie, Philipps-Universität Marburg

Introduction:

Limits in fossil energy carriers like oil and coal and increasing renunciation of nuclear energy stir up the demand for alternative and renewable or even unlimited energy sources. Among those solar energy is playing an increasingly important role. Since 1990 the power generation from solar energy shows a tremendous boost. In 2009 the amount of electrical power generated from solar cells was still one third of the corresponding production from hydrodynamic energy. In 2011 solar energy outran hydrodynamic power.[1]

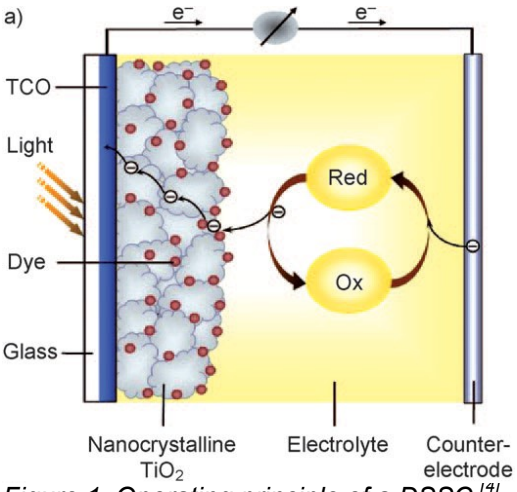

Figure 1. Operating principle of a DSSC.[4]

While photovoltaic cells depend on the cost demanding synthesis of pure silicon, dye-sensitised solar cells (DSSCs)[2] present an affordable alternative. With a power conversion efficiency of 15%[3] recent DSSC prototypes actually rival values of conventional solar cells. Still there is great potential for improvement regarding production costs and long term stability.

The operating principle of a DSSC is depicted in Figure 1.[4] A photoactive dye is absorbed onto a porous Titanium dioxide film. If the dye molecules are excited by sunlight an electron is transferred to the TiO_2 conduction band and from there to the anode consisting of a transparent conducting oxide (TCO). After transport of the electron to the counter electrode it will reduce the oxidised species of a redox couple. The reduced species diffuses to the dye anode where it reduces the dye molecule thereby returning to its oxidised form.

Results:

In the frame of my PhD research within the GRK 1782 I am focusing on the development of alternative redox couples -the traditional I^-/I_3^- couple suffers from severe disadvantages- thereby facilitating the exciton dissociation into mobile electrons and holes at the TiO_2 semiconductor surface. [5] (**A**) First objective is the synthesis of cobalt complexes with N,N-chelate ligands possessing NH-acidic functions. These can be deprotonated thereby leading to complexes with a decreased total charge compared to cobalt bipyridine complexes which have already been employed as redox mediators.[6] (**B**) Additionally I am concerned with the development of novel redox active anions which might be employed as counter ions to the classical, positively charged cobalt complexes.

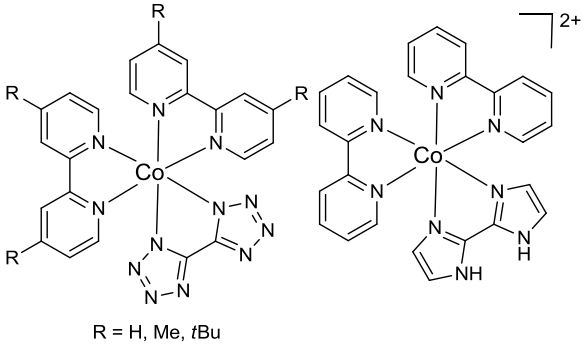

Figure 2. Cobalt complexes with dianionic ligands.

(**A**) Cobalt complexes bearing 5,5'-bistetrazole and 2,2'-bisimidazole ligands among bipyridine ligands have been prepared and fully characterised (Figure 2).[7,8] The 5,5'-bistetrazole complexes turned out to be very little soluble in common solvents, though. The solubility could only be enhanced by introducing bulky *tert*-butyl groups on the bipyridine ligands. Cyclic voltammetry experiments

showed that the compounds do not exhibit a well reversible redox behaviour.
Cobalt complexes with tetrazolyl-pyridine and imidazolyl-pyridine[8] ligands (Figure 3) have

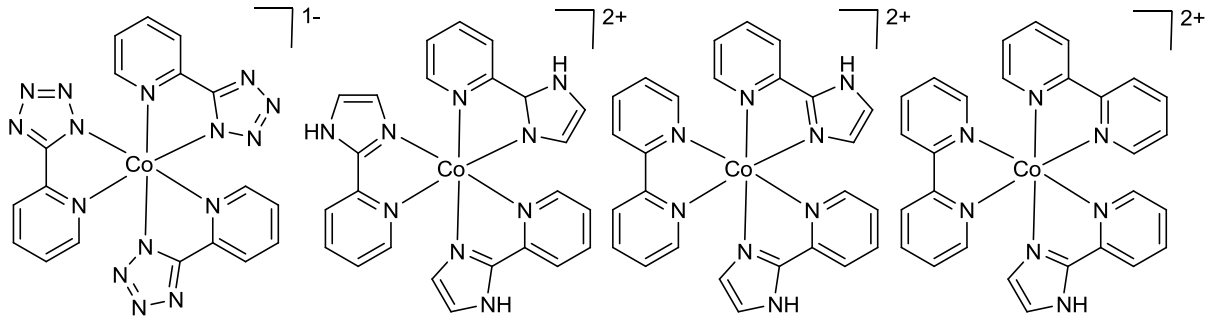

Figure 3. Tetrazolyl-pyridine and imidazolyl-pyridine cobalt complexes.

been synthesised and investigated in order to tune their redox potential. The tetrazolyl-pyridine complexes proved to be poorly soluble, complicating synthesis as well as characterisation. These compounds were therefore no longer pursued. The imidazolyl-pyridine complexes were readily accessible. During the detailed investigation of the complexes it turned out that the mixed ligand complexes reveal a fast intermolecular ligand exchange process at room temperature, which leads to a statistical ligand distribution. This could be shown by ^{1}H-NMR and ESI-MS experiments. Switching to cobalt(III) complexes that are in general considerably less prone to ligand exchange reactions did not lead to success as even at those complexes very fast ligand exchange already took place at room temperature. Very fast ligand exchange could be demonstrated between pure tris(bipyridine)cobalt(III)-hexafluorophosphate and pure tris(imidazolyl-pyridine)-cobalt(III)-hexafluorophosphate in an acetonitril solution at room temperature.
(**B**) The synthesis of redoxactive anions based on boron compounds with quinoide ligands has proven very difficult. Reactions starting from a variety of boron precursors (including BH_3, $LiBH_4$, BMe_3, $B(OMe)_3$, BF_3, BCl_3) did not lead to success. Most promising is the reaction between $LiBF_4$ and the corresponding OH-acidic ligand and reaction aids for deprotonating the OH moiety. Under these conditions product fragments could be observed in mass spectra.

Outlook:

In future the focus will lie on tridentate partly NH-acidic ligands. Despite the fact, that the coordination with three groups will considerably decrease the speed of ligand exchange, it will be possible to create homoleptic complexes where a ligand exchange between complexes is indifferent. 2,4-Dipyridyl-pyrrole and 2,5-bisimidazolyl-pyridine are among the anticipated ligands.
Experiments concerning redox active borates as anionic redox mediators will mainly focus on $LiBF_4$ and potentially other BF_4 salts as a starting material. Main objective is the isolation of the products which were only observed in mass spectra so far.

---

[1] Bundesministerium für Umwelt, Naturschutz und Reaktorsicherheit, *Erneuerbare Energien in Zahlen*, http://www.erneuerbare-energien.de/fileadmin/Daten_EE/Dokumente__PDFs_/20130114_BMU_EEiZ _Herbst12.pdf, accessed 05.08.2013.
[2] B. O'Regan, M. Grätzel, *Nature* **1991**, *353*, 737–740.
[3] Press release of the EPFL (11.07.2013): http://actu.epfl.ch/news/dye-sensitized-solar-cells-rival-conventional-ce-2/, accessed on 06.08.2013.
[4] A. Mishra, M. K. R. Fischer, P. Bäuerle, *Angew. Chem.* **2009**, *121*, 2510–2536.
[5] G. Boschloo and A. Hagfeldt, *Acc. Chem. Res.* **2009**, *42*, 1819–1826.
[6] T. W. Hamann, *Dalton Trans.* **2012**, *41*, 3111–3115.
[7] Y. Asfaha, *Bachelorarbeit*, Philipps-Universität Marburg, **2012**, Betreuer: L. H. Finger.
[8] S. Ullrich, *Bachelorarbeit*, Philipps-Universität Marburg, **2013**, Betreuer: L. H. Finger.

Hydrazine based amidine ligand systems: Precursors for vapour phase epitaxy of III-V semiconductors and metals

K. Schlechter, J. Sundermeyer

Philipps-University Marburg, Department of Chemistry, Hans-Meerwein-Straße, 35032 Marburg

Deprotonated amidines are versatile ligands and find applications in various areas such as catalysts for polymerisation and hydroamination[1] and precursors for VPE processes[1,2] (VPE, vapour phase epitaxy). Our goal is to investigate the so far unexplored coordination chemistry of *N,N'*-bis(diorganoamido)-substituted amidines and guanidines, especially of those derived from *1,1*-dimethylhydrazine, which can be synthesised by a condensation reaction of the dialkylhydrazine with the corresponding starting materials.

Up to now, three different types of ligands have been developed, a formamidin **1**, acetamidines **2a+2b** and guanidines **3a+3b**. They can be synthesised from triazine,[3] acetimido compounds[4] and thiourea or phosgene iminium chloride, respectively.

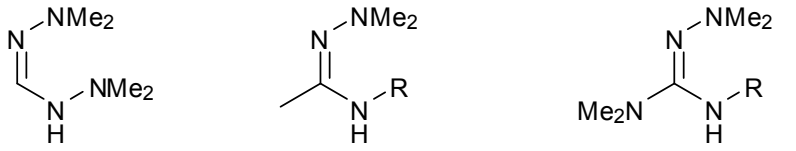

1: Hbdmf

2a: R=Me Hdama
2b: R=NMe_2 Hbdma

3a: R=Me Hdatg
3b: R=NMe_2 Hbdmg

Fig.1: synthesised ligands.

With the amidine ligands group 13 alkyl and hydrid complexes, homoleptic and heteroleptic d-block metal and metal halide complexes have been synthesised. The XRD structures of the analysed complexes have an unusual long *N-N*-bond within the five-membered ring, which represents a rated break point during CVD processes.

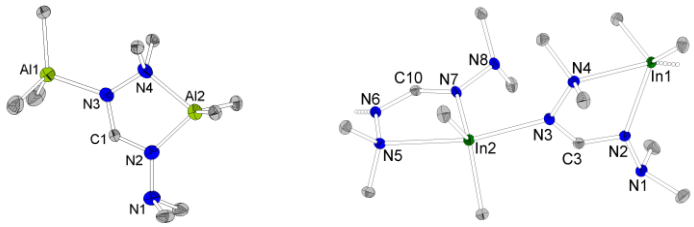

Fig.2: XRD structures of [$AlMe_3${$Al(bdmf)Me_2$}-κN] and [$In(bdmf)Me_2$].

In the future the syntheses of several more d-block and main group complexes are planned. All the compounds will be characterised by TGA and DSC analysis in an inert atmosphere. Following this, a few selected samples will be synthesised in larger quantity to be tested as VPE precursor in cooperation with the Stolz/Volz group.
The reaction of the electron rich amidine and guanidine ligands with group 13 alkyls or hydrides leads to potential precursors for VPE of III-V semiconductors. Deprotonation of the

ligands using KHMDS gives the potassium salts. These complexes can undergo a salt elimination with metal chlorides to synthesise various metal complexes, which might be used for VPE of metals.[5]

References

[1] F. Edelmann, *Chem. Soc. Rev.* **2009**, *38*, 2253-2268.
[2] H. Wang, R. G. Gordon, R. Alvis, R. M. Ulfig, *Chem. Vap. Dep.* **2009**, *15*, 312-319.
[3] C. Grundmann, A. Kreutzberger, *J. Am. Chem. Soc.* **1957**, *79*, 2839-2843.
[4] R. F. Smith, R. R. Soelch, T. P. Feltz, M. J. Martinelli, S. M. Geer, *J. Heterocycl. Chem.* **1981,** *18,* 319-325.
[5] W. Schorn, *Dissertation*, Philipps-Universität Marburg **2012**.

Quantum chemical investigations on the electronic structure of III/V-semiconductors for the computation of optical properties and on dynamical properties of the MOVPE process

Phil Rosenow, Ralf Tonner

Faculty of Chemistry and Material Sciences Center, Philipps-Universität Marburg

Introduction

This research evolves around the topic of III/V-semiconductor laser devices on top of silicon circuit structures or, in general, III/V-semiconductors grown on silicon. To research goals are connected with this: the computation of *ab initio* electronic structures of the laser material, the quaternary III/V-compound Ga(NAsP), and a better understanding of the reactions in the MOVPE-process used to grow GaP on silicon. The first part is to be used as a starting point for the computation of lasing properties in the group of Stephan Koch. Hereby, density functional theory is employed for the computation of band structures. The latter part is supposed to shed light on the atomistic and dynamical properties of the processes governing the MOVPE-procedure in close cooperation with Andreas Stegmüller. Chemical reactions occurring in the MOVPE process will be investigated using *ab initio* molecular dynamics. As a prerequisite for adsorption studies, the hydrogenation of the surface under MOVPE conditions must be investigated first. Computations are carried out using the VASP code.[1]

Results

Electronic structure of quaternary III/V-semiconductors – The band structure of the test system GaAs has been computed using density functional theory in the generalized gradient approximation with the PBE[2] functional and with the HSE06[3] hybrid functional. For comparison, the GW-approximation[4] has been applied as well. All methods underestimate the experimental band gap of 1.52 eV to different extent.[5] While HSE06 and GW yield reasonable results (1.14/1.07 eV), PBE is clearly off-limits (0.33 eV). In order to transfer the results to the theoretical semiconductor physics group in a useful way, wavefunction data has to be read out. This is currently underway and closing completion.

Thermodynamic properties of the Si(001)(2x1)-surface – The thermodynamics of hydrogen adsorption on the Si(001)-surface under MOVPE-conditions have been computed for various temperatures by employing surface phonons. Convergence with respect to slab thickness and supercell size is an issue yet to be resolved.

Dynamics of the adsorption of GaP-precursors on the Si(001)(2x1)-surface – Considering the importance of defect structures on the reactivity of surfaces, especially steps, surface cells containing no steps, a single step and a double step have been constructed for the hydrogenated (2x1)- and clean (4x2)-surface. These will be used in following adsorption studies. A remarkable feature occurs at steps on clean surfaces, when the dimers on the higher lying plateau are perpendicular to the step. In this case, the step atoms are dislocated from bulk positions in a way similar to dimers on the surface. Inspection of the charge density on these steps shows the same characteristics as for dimers, too (see figure 1).

Conclusions

Electronic structure of quaternary III/V-semiconductors – In the light of the results so far, the SE06 hybrid functional will be the method of choice for studies of the Ga(NAsP) laser material, offering sufficient accuracy for reasonable computational cost. The actual feasibility

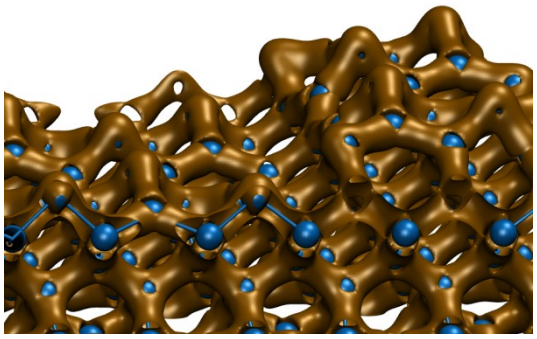

Fig.1: Charge density at a double step on the clean Si(001)(4x2) surface.

of the approach used here will be determined once the connection to the collaborators has been established.

Thermodynamic properties of the Si(001)(2x1)-surface – The aforementioned lack of convergence makes it impossible to draw unambiguous conclusions at this point. With due care, it can be assumed that the silicon surface is dehydrogenated between “low” (400°C) and “high” (675°C) temperature MOVPE operation conditions.

Dynamics of the adsorption of GaP-precursors on the Si(001)(2x1)-surface – Both the structural and electronic observations on surface steps at clean surfaces (with higher dimers perpendicular to the step) suggest a mechanism similar to the formation of dimers on the surface, where electron density is transferred from the “submerged” to the “elevated” dimer atom. This should have implications for the reactivity of steps of this kind. Furthermore, this implies that in order to get a picture of reactions occurring at steps, it is important to consider the orientation of the step with respect to the dimers.

Outlook

Electronic structure of quaternary III/V-semiconductors – Transfer of *ab initio* results to the collaborators will be realized in the near future, allowing for the calculation of optical properties based on these data. Once this connection has been established for the test system GaAs, actual production calculations for the laser material Ga(NAsP) can be performed. Owing to the structure of the target device, a model system will be used, the base of which is matched to GaP, while the height of the unit cell is relaxed under these strained conditions. The composition of the unit cell can be chosen to reflect the composition of the real material.

Thermodynamic properties of the Si(001)(2x1)-surface – Further studies are clearly necessary in order to resolve convergence issues. The used surface model as well as the accuracy of the computations will be investigated.

Dynamics of the adsorption of GaP-precursors on the Si(001)(2x1)-surface – The surface cells constructed so far, as well as possible other cells, will be used in molecular dynamics studies of the adsorption process. The surface will be initialized with a temperature mimicking experimental conditions while the precursors will be sent on a trajectory towards the surface, so that surface reactions can be simulated under well controlled parameters.

References

[1] G. Kresse, J. Hafner, *Phys. Rev B* **47**, 558 (1993); G. Kresse, J. Hafner, *Phys. Rev. B* **49**, 14251 (1994); G. Kresse, J. Furthmüller, *Comput. Mat. Sci.* **6**, 15 (1996); G. Kresse, J. Furthmüller, *Phys. Rev. B* **54**, 11169 (1996). [2] J. P. Perdew, K. Burke, M. Ernzerhof, *Phys. Rev. Lett.* **77**, 3865 (1996). [3] A. V. Krukau, O. A. Vydrov, A. F. Izmaylov, G. E. Scuseria, *J. Chem. Phys.* **125**, 224106 (2006). [4] L. Hedin, *Phys. Rev.* **139**, 796 (1965). [5] Kim et al., *Phys. Rev. B* **82**, 205212 (2010).

Ab initio study of MOVPE Gas Phase Decomposition Mechanisms

Andreas Stegmüller and Ralf Tonner

Department of Chemistry, Philipps-Universität Marburg

Introduction

The simulation of CVD processes has been undertaken by various quantum chemical methods.[1] In this first part of the GRK research project the specific gas phase decomposition chemistry of a triethylgallane (TEG) and *tert*-butylphosphine (TBP) MOVPE system was investigated with quantum chemical calculations.

In the focus of this investigation lies the identification of elementary decomposition reactions of the precursors and the evaluation of event probabilities under realistic thermodynamic conditions (H_2 atmosphere, 50 mbar total pressure, temperatures of 400 to 675 °C). This will be complemented by mechanism analyses and energy barriers, which will provide the necessary elementary process rates for a larger-scale simulation involving surface and GaP thin layer growth processes.[2]

Within the reaction catalogue of decompositions there were four unimolecular mechanism classes identified for each source species and three bimolecular mechanisms, respectively. The elementary steps were combined in decomposition networks for the individual precursors. On the basis of the reactions' thermodynamic properties it was possible to formulate different pathways leading to small decomposition products.

From those combined thermodynamic pathways relevant elimination steps were chosen for mechanistic studies to unveil reaction kinetics. Among the criteria for this choice are the thermodynamic spontaneity of a reaction, the probability of the reaction educts to collide and undergo a reaction, etc. (see approximations below).

Results

Efficient DFT methods (GGA functional PBE-D3[3]) were applied (with a correction for non-covalent dispersion interactions) alongside highly accurate wave function based methods like MP2 and CCSD(T) as measure for the accuracy (which proved the match well, especially for reaction energies of exclusively non-radical compounds). The def2-TZVPP triple zeta basis set was used throughout.[4]

For the modeling and evaluation of the MOVPE gas phase reactivity, a number of approximations had to be introduced in this study including the following statements:

- ab initio calculations were performed, assuming ideal gas distributions and Boltzmann-distributed partition functions for thermodynamic corrections,
- low partial pressures of precursor compounds in the H_2 carrier gas, which allows to neglect the formation of III-V adducts or the occurrence of alkyl (radical) recombinations in the gas phase (with the exception of reactions with the H radical, which thermally desorbs from the substrate at 480 to 580 °C [5] and reactions with the omnipresent H_2),
- no heterogeneous effects with the reactor walls or the substrate surface were considered (so far). The last issue will be addressed in a future study, as the overall decomposition rate will be prominently determined by those surface-assisted reactions.

The number of pathways to be formulated on the basis of thermodynamic favorability was small, fortunately, however the scientific community is invited to unveil any relevant process that might complement those networks (comp. Fig. 1).

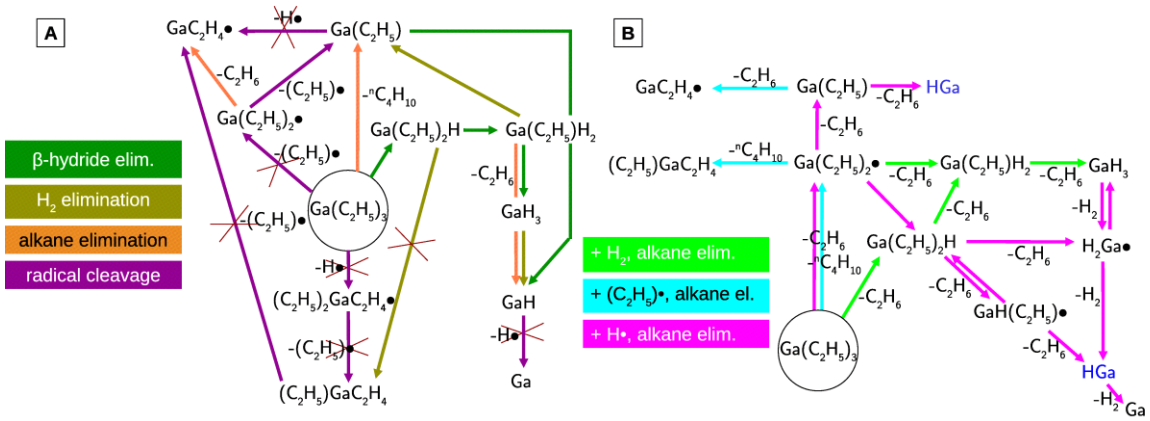

Fig.1: Decomposition networks indicating accessible elementary steps for uni- (A) and bimolecular (B) reactions as calculated by the Free Reation Energy, ΔG, at 400 °C (PBE/TZ) for TEG.

Conclusions

The decomposition networks show that, formally, atomic Ga and P can result from gas phase thermal decompositions. Following the thermodynamic argument more rigorously, most formal pathways appear unlikely to occur (as indicated by endothermicity at 400 °C: crossed in Fig. 1). Moreover, even exothermic processes possess large barriers, hence only a small number of compounds can be determined likely candidates for adsorption. These are mainly the initial precursors and potentially GaH_3 (mono-gallane) and GaH (gallium hydride).

For an understanding of the MOVPE process, the next questions to answer already involve investigations of the surface (e.g. if and why Ga seems to be more stable at direct contact to the Si substrate as opposed to P species; or whether P adsorbs as intact molecule and tends to desorb easily from the Si substrate). The investigation of gas phase decompositions, however, showed class-dependent trends in thermodynamics as well as kinetics. Those can be utilized twofold: firstly, to chemically understand the individual mechanistic steps of the eliminations and, secondly, as categorization help for computationally more demanding investigations of similar mechanisms (e.g. surface-assisted reactivity calculations in periodic models). Furthermore, the fundamental differences in the β-hydrogen elimination mechanisms of group 15 with respect to group 13 *tert*-butyl compounds was investigated applying techniques of quantum chemical bonding analysis.

Outlook

In the second part of this project elimination mechanisms on the surface will be studied and compared to equivalent molecular mechanisms. This will be realized by applying the NEB[6] method and/or adaptive kinetic Monte Carlo[7].

Further surface elementary processes that need to be investigated include diffusion and layer growth processes. Particularly important are stabilities of individual adsorbates at relevant sites, especially for multi-adsorbate configurations up to complete (mono)layers of Ga, P and GaP.

References

[1] a) A. Y. Timoshkin and H. F. Schaefer III, J. Phys. Chem. C, 112, 2008, 1381636. b) B. Mondal et al., J. Phys. Chem. A, 2010, 114, 5016–25. c) J. Schäfer et al., Chem. Phys. Lett., 2000, 319, 477–81. d) R. Schmid and D. Basting, J. Phys. Chem. A, 2005, 109, 2623–30.
[2] a) K. Reuter, in Modeling Heterogeneous Catalytic Reactions: From the Molecular Process to the Technical System, ed. O. Deutschmann, Wiley-VCH, Weinberg, 2009. b) M. Scheffler et al., Phys. Rev. B, 2010, 82, 214417. [3] a) J. P. Perdew, K. Burke and M. Ernzerhof, Phys. Rev. Lett., 1996, 77, 3865–3868. b) S. Grimme et al., J. Comp. Chem., 2011, 32, 1456-65.
[4] F. Weigend and R. Ahlrichs, Phys. Chem. Chem. Phys., 2005, 7, 3297–305. [5] K. Kohse-Höinghaus et al., J. Amer. Soc. Mass Spec., 2008, 19, 947–54. [6] G. Henkelman et al., J. Chem. Phys., 2000, 113, 9901. [7] G. Henkelman et al., J. Chem. Phys., 2008, 129, 114104.

Evaluation of Ga(AsBi) HAADF-images via the Voronoi diagram

Nikolai Knaub

Faculty of Physics and Material Sciences Center, Philipps-Universität Marburg

It is known, that incorporating small amounts of Bi in III/V semiconductors (such as GaAs) has a huge influence on the energetic position of the valence bands, mainly also of the spin-orbit split-off band [1]. This reduces the Auger-loss processes which leads to less heat production in a semiconductor. Therefore, dilute bismides such as Ga(AsBi) are promising materials for optical and electronical devices. For a sufficent incorporation of Bi in GaAs, the growth temperature of MOVPE (metal organic vapour phase epitaxy)-grown samples has to be low, typically between 375° C and 450° C [2]. Because of such relatively low growth temperatures point defects, such as Bi antisites or even Bi-clustering and thus a non statistical randomly distribution of the Bi atoms, can arise and influence the crystal structure.

For the characterization of Ga(AsBi) layers grown on GaAs, I used the scanning transmission electron microscopy (STEM) high angle annular dark field (HAADF) technique on conventionnally prepared cross-section TEM samples. Since the HAADF method is based on the interaction of the electrons with the nuclei (Rutherford-scattering), it allows to measure the scattering of the electrons in high angles (typically 50-120 mrad) by a scintillator material based annular detector. Since the measured intensity is approximately proportional to the square of the atomic number Z a clear distinction of different material systems such as GaAs and Ga(AsBi) and especially the investigation of the interfaces is possible. The imaging was performed in a double spherical aberration corrected JEOL JEM 2200 FS at an acceleration voltage of 200 kV. The probe aberration correction allows an investigation of the sample on an atomic scale and therefore an analysis of each particular atomic column.

The evaluation of the HAADF measurements was first performed with a Voronoi diagram based method by measuring the mean intensity of each atomic column. Thereto, the experimental image is divided in particular regions (for example Voronoi cells), where each cell contains one atomic column and a certain amount of pixels (figure 1a & 1b). One derives the mean intensity of each cell and hence of each atomic column by normalizing the cell intensity by the pixel number. The big advantage of this method is the possibility to separate the group III and group V sublattices in the experimental and simulated HAADF images by the construction of such a diagram. Thus one can distinguish between atoms with nearly the same atomic number Z, such as Ga and As. Since one has the mean intensity of each atomic column it is possible to plot the counted column intensities and due to the sublattice separation it is also possible to determine the composition of each atomic column. Thus one can investigate the influence of Bi on the crystal structure by evaluation of the group V sublattice intensities only. With further evaluation processes it came out, that the area of a Voronoi cell is to coarse for a significant evaluation of the seperated group III and group V sublattices due to a bad signal to noise ration. For that reason I decided to integrate over a certain radius, which is one quarter of the nearest neighbour distance between two atomic columns. Furthermore I showed, that the measured intensity and therefore the intensity distribution depends strongly on the chosen inner detector angle of the annular dark field detector. Since smaller angles lead more to a strain contrast in the image rather than to Z-contrast, higher angles (above 50 mrad) should be the angles of the choice for a quantitative analysis of the investigated material.

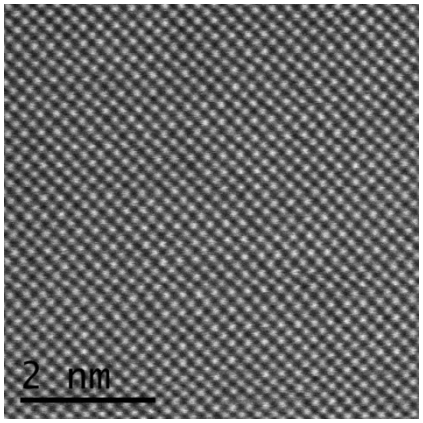

Figure 1(a): STEM HAADF image of a MOVPE grown Ga(AsBi) quantum well in [010] direction.

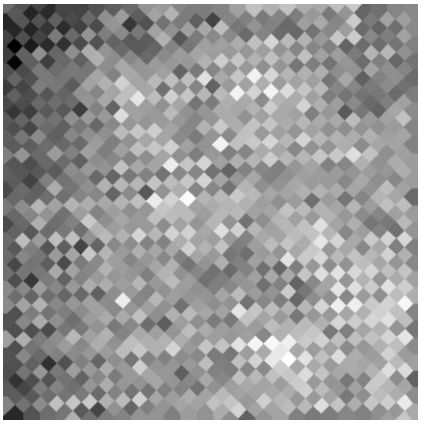

Figure 1(b): A mean intensity map (Voronoi map) of figure 1(a), the brighter cells represent As columns occupied by Bi atoms.

These first results show on the one hand the need of an aberration corrected STEM to analyze such complex materials as Ga(AsBi) on an atomic scale, so to say to analyze each particular atom column. On the other hand the Voronoi diagram method could be succesfully demonstrated on Ga(AsBi), which allows to see the occupation of Bi-atoms on As-atom collumns and furthermore allows the seperation of group III and group V sublattices. This gives the possibility for a precise quantification of the investigated material.

More evaluation will be done with the Voronoi method, but instead of the Voronoi cell I will use the mentioned integration radius of one quarter neighbour distance of two atomic columns to get a better signal to noise ratio. Furthermore HAADF simulations must be considered for comparison of experiment and simulation as well as for evaluation of the intensity statistics and thus the quantification of the measured images. Also planned is to apply this Voronoi diagram approach on other material systems, such as Ga(NAs) or even on the quaternary material Ga(NAsBi).

[1] Alberi et al., Applied Physics Letters 91(5), 051909 (2007)
[2] Ludewig et al., Journal of Crystal Growth 370, p.186–190 (2012)

MOVPE Growth of Dilute Bismide Ga(AsBi) Quantum Well Structures for High Efficiency IR Laser Devices

P. Ludewig, N. Knaub, Z. Bushell, L. Nattermann, E. Sterzer, W. Stolz, K. Volz

Faculty of Physics and Material Sciences Center, Philipps-Universität Marburg

Dilute bismide Ga(AsBi) based lasers diodes are promising candidates for high efficiency IR light sources. The incorporation of only a small amount of Bi into GaAs decreases the temperature sensitivity of the emission wavelength compared to conventional III/V semiconductors hence less cooling of the devices is needed. Furthermore, if the Bi content is above 10.5 %, the spin-orbit splitting becomes larger than the bandgap which is due to the band anticrossing in the valance band. In this case auger loss processes could be suppressed leading to higher efficiencies and less heating of the devices. However, Ga(AsBi) is highly metastable which leads to segregation of bismide at the surface and the formation of metallic droplets during growth. In order to incorporate a significant amount of Bi into GaAs low growth temperatures are required and all growth parameters need to be adjusted very carefully.

Ga(AsBi)/GaAs quantum well (QW) and bulk structures were grown by metal organic vapor phase epitaxy (MOVPE) on exact GaAs (001) substrates. All liquid precursors as triethylgallium (TEGa), trimethylaluminum (TMAl), tertiarybutylarsine (TBAs) and trimethylbismuth (TMBi) were used to enable growth temperature as low as 375 °C to 450 °C. The structure of the samples was investigated by as scanning transmission electron microscopy (STEM), high resolution X-ray diffraction (HR-XRD) and atomic force microscopy (AFM). The optical properties were studied by room temperature photoluminescence (PL) measurements.

If all parameters are adjusted carefully Ga(AsBi) layers with Bi fractions up to 5% in good quality can be realized without any formation of metallic droplets. It was found, that the incorporation of Bi into GaAs is limited depending on the applied growth temperature and growth rate and can be influenced by the V/V ratio. Surplus Bi then segregates to the surface and can incorporate into subsequent layers or form metallic droplets if it is not evaporated by a growth interruption at higher temperatures. All samples show a significant PL signal already after growth which can further be improved by annealing at temperatures between 600 °C and 700 °C. The PL peak shifts by about 80 meV / % Bi which is in a good agreement with the theory. The introduction of (AlGa)As barriers grown at 625 °C improves the electronic confinement of the Ga(AsBi) quantum wells compared to pure GaAs barriers and therefore allows the growth of laser diodes. First experiments on a $Ga(AsBi_{0.022})$/(AlGa)As SQW device show promising threshold currents in the range of 800 mA/cm² at an emission wavelength of 950 nm.

However the growth of this new material system by MOVPE at these relatively low temperatures is still very challenging and not yet fully understood. In future more experiments need to be carried out to get a more detailed understanding of the Bi incorporation mechanism which will help to further increase the Bi fraction of the crystals. In addition Ga(AsBi) laser structures with Bi > 4% will be grown and the demonstration of the reduced temperature sensitivity of these devices is planned.

Preparation and characterization of phenylphosphonic acid self-assembled monolayers on ZnO substrates

Alexandra Ostapenko, Gregor Witte

Molecular solid state physics, Philipps-University Marburg, Germany

Introduction

Semiconductors with chemically modified surfaces by covalently bound molecular layers are promising materials in developing electronic devices and sensors. The strategy comprises obtaining higher efficiencies from organic photovoltaic and photoelectrochemical cells and in many other applications since atomic and electronic structure of semiconductor surfaces can be tuned by variations of adsorption parameters and adsorbate reactivity [1]. In particular, semiconducting properties of metal oxides as organic-inorganic hybrid structures for photovoltaics is of great interest. Zinc oxide is a transparent metal oxide that has gathered significant interest as electron-selective/electron-transport material for solar cells and light-emitting diodes (LEDs) and in sensor applications. In such application like dye sensitized solar cells [2] electronic coupling at the organic/inorganic heterojunction is significant since the charge transport across the heterojunction is decisive for charge carrier separation. This project is dealing with the linkage of molecular chromophores on oxide semiconductors. As a first step the linkage has been studied by characterising the anchoring mechanism of self-assembled monolayers on single crystalline oxides. In contrast to the commonly used thiol-based anchoring on metals such as gold or silanes coupled to silicon oxide only a few systematic studies have been reported concerning the anchoring on metal oxides. In this study we have chosen phenylphosphonic acid (PPA) for the fabrication of self-assembled layers because they are molecules with the simplest aromatic backbone (Figure 1) holding distinct signature in NEXAFS spectra that can be easily separated from carbon contamination. One particular aspect is to unravel the chemical linkage of phosphonic acids on metal oxide surfaces i.e. formation of mono-, bi- or tri-dentate species. Another important aspect, which has not been properly considered until now, is the influence of substrate defects such as oxygen vacancies and other impurities on the binding efficiency, the resulting packing density and the molecular orientation since most previous studies were performed on polycrystalline samples [3].

Results and conclusions

To address the influence of surface chemical termination SAMs were prepared on different ZnO single crystal surfaces, comprising both polar ZnO (000-1)-O, ZnO (0001)-Zn as mixed terminated ZnO (10-10) surfaces obtained by previously established procedure [4]. Adsorption of PPA was studied on bare as well as OH-terminated ZnO substrates prepared by NaOH dip before immersion in SAMs solution. To control preparation of the substrate experiments such as atomic force microscopy (AFM), low energy electron diffraction (LEED) were carried out. By means of thermal desorption spectroscopy (TDS) the binding strength of molecules was determined. Contact angle measurements were used to characterize chemical surface modification. To characterize the adsorption kinetics and thermal stability of PPA-based films on zinc oxide surfaces chemical anchoring mechanism was studied by means of high resolution XPS and the molecular orientation was determined by NEXAFS measurements. According to results of XPS spectroscopy PPA forms well-ordered thin films.

The largest coverage is achieved for rough surfaces that have been created in a controlled way by ion sputtering. This behavior is assigned to more strongly bond at defects like steps or kicks anchor groups. A quantitative analysis of dichroism of the π^* excitations (Figure 2.) in the NEXAFS spectra yields an orientation of the aromatic backbone planes of 15° with respect to the surface normal. These quantities are also compared with SAMs prepared on powder samples.

Outlook

To expand the knowledge about adsorption of SAMs on transparent metal oxides it is planned to use another combination of molecules (phosphonic acid with other functional groups and carboxylic acid) as well as other types of metal oxides (TiO_2 as it is widely used in photovoltaic and photocatalytic applications). However in contrast to ZnO titanium dioxide is more difficult to be prepared due to its high reactivity which requires careful sample treatment and avoiding contact with air. Therefore the preparation procedure must be optimized aiming to prevent presence of defect sites on the surface.

[1] Yaffe O, et al., Nano Lett, 9, 2390–2394 (2009)
[2] Hagfeldtet A. al., Chemical Reviews, 110, 6595 (2010)
[3] Gliboff M, et al., Langmuir, 29, 2166-2174 (2013)
[4] J. Goetzen and G. Witte, Applied Surface Science, 258, 10144 - 10147 (2012)

Figure 1. Scheme of phenylphosphonic acid

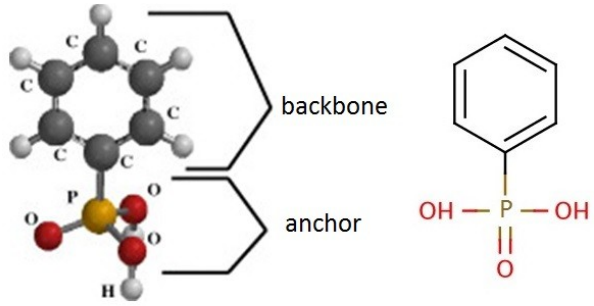

Figure 2. NEXAFS spectra of phenylphosphonic acid adsorbed on ZnO single crystal O-terminated differently treaded surface: a) rough surface; b) OH- modified rough surface; c) well-ordered surface; d) OH- modified well-ordered surface

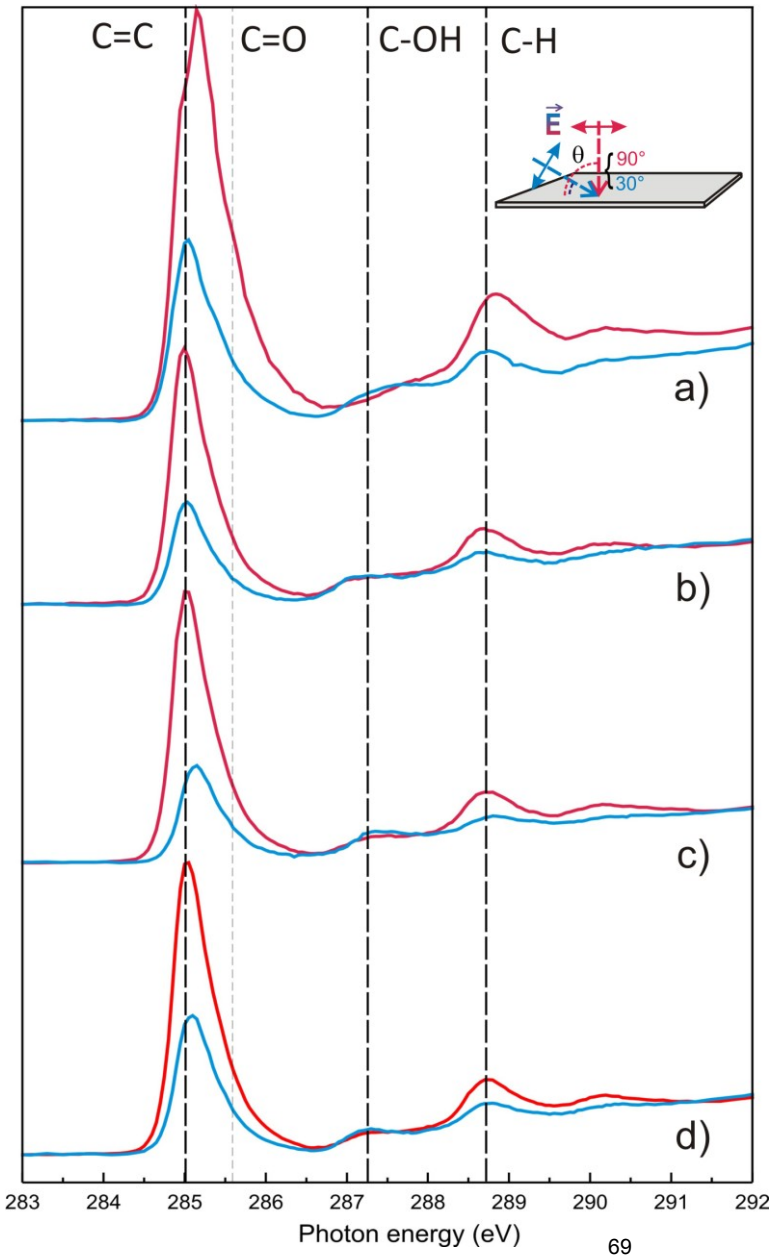

SELECTIVE NUCLEATION OF ORGANIC SEMICONDUCTORS

André Pick, Prof. Dr. Gregor Witte

Faculty of Physcics, Molecular Solids, Philipps University Marburg

Introduction

In order to build up organic electronic devices, control of crystallization of the organic semiconductors is cruical. In fact, one has to tune parameters in a way that size, shape, density and orientation of single crystals are determined. The latter aspect is of importance, as the structure of molecule-based crystals exhibits anisotropies, so that e.g. optoelectronic properties are dependent on the crystallographic directions. As the ultimate goal one could imagine growing crystals polymorphism-selectively.
Single-crystal transistor arrays have been fabricated using several polycyclic aromatic hydrocarbons [1]. To achieve such a lateral structured growth-mode, microcontact-printing has often been used, thus being able to create domains of nucleation by printing self-assembled monolayers on the micron-scale.
In this research we are focussing on the nucleation itself: Our aim is to figure out which microscopic mechanism is responsible for site-selectivity, as in the literature several suggestions were made and the situation remains unclear. To get this information, we have choosen the system of aliphatic thiols on gold-surfaces, where we deposit Perylene under UHV-conditions.

Results

First of all, we analyzed the influence of substrate-roughness of a SAM-covered Au-surface on the growth of Perylene. Therefore we used Au(111)/Mica-sheets (local atomic flatness on the 100nm-scale) and compared them with polycrystalline films on silicon-wafers (Au-clusters, ~50nm in diameter).
By doing this with a SAM of 1-Octadecanethiol, one can observe a significant difference concerning size, shape and density of crystals. While the crystals on the Au(111)/Mica-sheets appear dendritic with lateral dimensions of ~50µm, those on the polycrystalline substrate are smaller (~1µm) and exhibit a squarisch morphology. The density of individual crystals on the polycrystalline surface is increased by far compared to the Au(111)-substrate. In the latter case, there are only a few crystals on $1cm^2$, while the density on the polycrystalline can reach $\sim 1/\mu m^2$.

In the second part of our study we varyied the chain length and the functional group of the SAM. Here we modified the surfaces with Butanethiol, Dodecanethiol, Octadecanethiol and Mercaptoundecanol. As we expected, no fundamental differences were observed. We assume that the packing density of the SAMs is modified by changing the functional group and thus influences the growth of perylene due to defects.

To achieve a lateral structured growth-mode we printed Octadacnethiol on the polycrystalline surface. The stamped regions acted as active domains for nucleation. Especially on thick films of the stamped material crystals grew in a defined fashion, making it also possible to

grow a crystal between two electrodes. As Octadecanethiol is a wax, it is not possible to study the growth on a homogenous covered surface, because the material tends to agglomorate. This led to the idea to use siliconeoil instead of low vapor-pressure thiols. Here the same site-selectivity could be observed. The main difference is that crystals are growing in a supersaturated oil-film, while growing ontop of the wax.

Conclusion

We have succesfully grown perylene selectively on an Au-substrate by stamping a thick film of a wax (Octadecanethiol) or an oil (siliconeoil). Both scenarios indicate that the interaction of the perylene-molecules to the substrate vanishes in the stamped regions. In the case of the oil the perylene is solved in it. By deposition from a Knudsen-Cell a continously supersaturated film is created where nucleation takes place.

Outlook

In the future, we will perform experiments on the diffusion of perylene on SAMs. This can be done either by depositing an amorph Perylene-film at lower temperatures and subsequent thawing or by varying the lattice constant of the silicone-stamp. Thus we should be able to adjust optimized conditions for site-selective single crystal growth.

References:

[1] Briseno et al.: Patterning Organic Single-Crystal Transisitor Arrays, *Nature* **2006**, 444, 913-917

Teilnehmer GRK-Seminar
vom 19. - 22.08.2013 in Hofheim

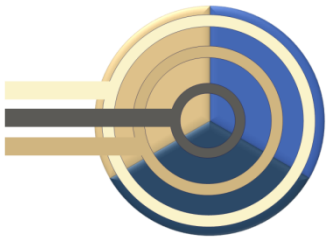

Stipendiat/Innen
Eußner, Jens
Knaub, Nikolai
Meyenburg, Ingo
Oelerich, Jan Oliver
Ostapenko, Alexandra
Prinzisky, Christian
Reutzel, Marcel
Rosenow, Phil
Werner, Katharina
Woscholski, Ronja

Kollegiat/Innen
Breddermann, Benjamin
Finger, Lars
Kaiser, Uwe
Leusmann, Eliza
Lipponer, Marcus
Ludewig, Peter
Pick, Andre
Rosemann, Nils
Sabir, Nadeem
Stegmüller, Andreas
Weinert, Bastian

Studentische Hilfskräfte
Bushell, Zoe
Gies, Sebastian
von Helden, Leonard
Nattermann, Lukas

Sonstige Teilnehmer/innen
Gries, Katharina, Dr.
Lippert, Sina

Betreuer/innen
Chatterjee, Sangam, Dr.
Dehnen, Stefanie, Prof. Dr.
Heimbrodt, Wolfram, Prof. Dr.
Parak, Wolfgang, Prof. Dr.
Sundermeyer, Jörg, Prof. Dr.
Tonner, Ralf, Dr.
Volz, Kerstin, Prof. Dr.
Witte, Gregor, Prof. Dr.